Control Engineering Practice 146 (2024) 105866

Contents lists available at ScienceDirect

Control Engineering Practice

journal homepage: www.elsevier.com/locate/conengprac

Control of the launch and recovery of small boats to a mothership in high sea states using sliding mode methods

Vikram Rout [a,1], Liam Vile [a,2], Christopher Edwards [a,*], Michael J. Belmont [a], Guang Li [b], Dominic Taunton [c]

[a] College of Engineering, Mathematics and Physical Sciences, University of Exeter, UK
[b] School of Engineering and Materials Science, Queen Mary, University of London, UK
[c] Faculty of Engineering and Physical Sciences, University of Southampton, UK

ARTICLE INFO

Keywords:
Launch and recovery
High sea states
Underactuated system
Crane
Sliding mode control
Integral sliding mode control

ABSTRACT

The launch and recovery (L&R) of a small vessel from a large mothership occurs in various settings, such as the rescue of stranded personnel, extraction of unmanned autonomous sea monitoring sensors and the deployment of rescue submersibles. L&R of a small vessel, from a large mothership, at high sea states is difficult and is often avoided for safety reasons. This paper proposes sliding mode controllers to automate the process involving a modified davit crane in which the suspension point is movable. This is the first time a robust control strategy has been used to tackle this specific maritime problem.

In this work, a second-order sliding mode controller is used to change the length of the cable during the recovery process and ensures that a pre-defined profile for the cable's length is followed. This controller alone proves to be sufficient for a safe recovery at low sea states. However, for higher sea states, the small vessel and mothership collide under certain circumstances. An integral sliding mode controller is introduced to adjust the crane's boom, which modifies the position of the suspension point, such that the oscillations of the small vessel are minimized. This controller aims to keep the distance between the mothership's hull and the centre of the small vessel at a constant value by adjusting the position of the crane's boom and reducing the swing angle. The overall control algorithm is found to be very effective, compared to the fixed boom case, ensuring that collisions do not occur under any of the tested configurations, and a safe distance is maintained between the mothership and the small vessel. The performance evaluation of the controller predicts that it will safely operate in rough sea states for any initial combination of swing angle and velocity, if a safe recovery can be carried out at a lower sea state for the same initial conditions.

1. Introduction

In calm water (i.e. up to sea state 3, where the wave height is between 0.5 m–1.25 m) the L&R process can be carried out by a trained operator using their experience and discretion. However, for higher sea states (4 and above, with wave heights greater than 1.25 m), despite the presence of experienced operators, the uncertain nature of the waves adds a significant amount of complexity to this process. This increases the danger to any personnel on the small vessel, and increases the possibility of damage to the mothership and the small vessel arising from collisions (see Figs. 1 and 2). The existing mechanisms for L&R can be broadly classified into three categories: ramps, intermediate capture devices (Hanyok & Smith, 2010), and cranes. This paper focuses on the use of cranes. L&R using cranes involves a diverse set of arrangements including side davits, boom, knuckle, extending, and A-frame cranes, and any other combination of a boom and winch (Büchel & Åkerlund, 2015; Hanyok & Smith, 2010; Jin, Wan, Liu, Peng, & Guo, 2016).

During a crane based launch or recovery process, the winch control operator has to deal with the oscillations of the small vessel and ensure that it does not capsize. The oscillations when the small boat is clear of the water during the recovery process can also result in collisions with the hull of the mothership causing damage to both the mothership and the small vessel. Oscillations of the small vessel is the major hindrance to safe L&R. The motivation behind this paper is to develop a control algorithm to aid crane operators and to partly automate the recovery process of the small vessel in high sea states, and to help determine the sea states and initial conditions for which recovery is viable. In this

* Corresponding author.
E-mail address: c.edwards@exeter.ac.uk (C. Edwards).

[1] Vikram Rout is an Early Stage Researcher funded by the Marie Skłodowska-Curie Grant #765579 - ConFlex.
[2] Liam Vile is supported by the EPSRC project EP/P022952/1.

https://doi.org/10.1016/j.conengprac.2024.105866
Received 27 June 2023; Received in revised form 21 December 2023; Accepted 19 January 2024

Fig. 1. Launch of a smaller vessel from a larger mothership using a davit (*Palfinger NPDS series fast rescue boat davits*, 2023).

Fig. 2. Capture of a smaller vessel with a stern cage on to the mothership (Fjelldal, 2017).

paper a modification to the traditional boom of the crane is considered. The boom position is assumed to be adjustable to enable lateral movement of the suspension point to reduce the oscillations of the small vessel. This modified crane is therefore similar to the telescopic boom crane (Hong & Shah, 2019). However a typical dynamic crane system is an underactuated system since the number of control variables is less than the degrees of freedom (Kim & Hong, 2019; Ngo, Nguyen, Nguyen, Tran, & Ha, 2017). There are many examples of engineering systems which are underactuated: some examples include submarines and VTOL (vertical takeoff and landing) aircraft which have 6DOF, but usually only 4 actuated variables in the form of thrust in one direction and torque control for angular orientation along each of the three axes (Hua, Hamel, Morin, & Samson, 2009; Roza & Maggiore, 2014). Other important examples of underactuated systems includes flexible joint robots and the cart–pole system, where a single control input is applied to a system with two degrees of freedom (Khan, Rsetam, Cao, & Man, 2022; Maalouf, Moog, Aoustin, & Li, 2015). The crane-small vessel assembly considered in this paper falls under Class III of the underactuated systems classification as delineated by Olfati-Saber (2001).

Typically, the primary goal of (any) crane control system is to minimize unwanted motions of the payload during transport from one location to another. Such motion can originate from the inertial forces of the payload itself, base excitations of the supporting structure (in this case, the mothership) or wind loads. In some situations the effect of the inertial forces can be mitigated by the crane operator performing the transport manoeuvres slowly. Control strategies for ameliorating the external excitations can be classified into open-loop and closed-loop control, and differ depending on the type of crane being used (gantry, rotary, boom crane etc.).

Open-loop control methods include input-shaping, where the crane operates along a pre-determined path (Hubbell, Koch, & McCormick, 1992; Parker, Petterson, Dohrmann, & Robinett, 1995; Takeuchi, Fujikawa, & Yamada, 1988). An acceleration profile for the crane is obtained such that the residual oscillations during transport of the payload are minimal. Another open-loop control method is optimal control where the velocity (Field, 1961) or acceleration (Beeston, 1969; Manson, 1982) profiles are optimized. The optimization can be based on minimizing oscillations or limited hoisting and transport time. Genetic algorithms have also been implemented for the optimization process (Kimiaghalam, Homaifar, & Bikdash, 1998). Zhang, Zhao, and Ding (2022) developed a data-driven optimal adaptive control scheme for a 2D overhead crane model to regulate the position of the crane and its swing. Their data-driven controller does not rely on prior knowledge of the dynamics of the system. Wu, Xu, Lei, and He (2020) used feed-forward compensation control for the 2D overhead crane system with uncertain disturbances (estimated using a nonlinear disturbance observer) by converting the model into a quasi-integrator-chain form. This was combined with a global SMC such that the nominal control performance of the controller was preserved.

Closed-loop crane control of ships has been studied by a wide number of researchers. Chin, Nayfeh, and Mook (2000) studied the factors affecting the large excitations of the payload when transferring it from one ship to another using a ship-mounted crane and highlighted the primary reasons as large wave amplitudes and small wave amplitudes near the resonance of the payload (Idres, Youssef, Mook, & Nayfeh, 2003). Fang, Wang, Sun, and Zhang (2014) developed a dynamic model of an offshore boom crane using the Euler–Lagrange method and studied the effects of the ship's motion on the swing angle of the payload. The controller was based on developing planned trajectories for the cable length and the luff angle,[3] and then developing a Sliding Mode Controller (SMC) to adhere to these trajectories. These actuated variables were also used to ensure that the un-actuated variable, the swing angle, goes to zero. The controller was shown to be very robust in the sense of not being affected by the disturbances resulting from ship motions. Sun, Fang, Chen, Fu, and Lu (2018) implemented a coordinate transformation to represent the disturbances in a different form to incorporate the ship's roll and heave motions as disturbances for the crane dynamics. They developed a closed-loop control method to stabilize the ship-mounted crane in the presence of roll and heave motions without any linearization or approximation of the non-linear dynamics of the system. Küchler, Mahl, Neupert, Schneider, and Sawodny (2011) used a prediction algorithm to obtain the vertical motion of the ship and then an inversion-based control algorithm was implemented to transport the payload and minimize the disturbances. Kim and Hong (2019) implemented an adaptive SMC with 4DOF control for an offshore container crane experiencing unknown disturbances. A sliding surface was determined to include the actuated and un-actuated variables. SMC was used with two adaptation laws for switching. The adaptation laws were used to compensate for the disturbances and minimize chattering around the sliding surface. They tested this control scheme for sudden and unknown disturbances like wind gusts, and found the controller to be robust in these conditions. The only mothership motions considered for producing the disturbances were roll and pitch. Chen and Sun (2021) developed a closed-loop output feedback control scheme for a 5 degree-of-freedom offshore crane system by considering the ship's yaw and roll motions.

Cao and Li (2020) produced a review paper focusing on the anti-swing controller characteristics for cranes onboard ships. Due to the additional degrees of freedom that exist for cranes on ships compared to land cranes, the control strategies vary immensely. This review compiled the antiswing control research into three types of cranes onboard of a ship: overhead, boom and tower cranes. The physical methods included using a tagline and rider block to change the pendulum's frequency, Maryland rigging, changing the pulley length, and

[3] Luff angle is the angle made by the crane's boom with its horizontal base.

the introduction of an active anti-pendulation arm. Researchers have focused on the development of control schemes for these systems. These can be categorized into linear control, feedback linearization, backstepping control, sliding mode control, energy-based feedback control and intelligent control. Bozkurt and Ertogan (2023) developed a control scheme for payload transfer between two ships in rough seas. This was based on the use of Particle Swarm Optimization to obtain the gains for Proportional–Integral–Derivative (PID) and Proportional–Derivative-Second Derivative control (PDD^2) systems. The PID controller was used to control the horizontal and vertical movement of the payload, while the PDD^2 method was used to control the swing of the payload. However, an extra telescopic boom was added to the main boom for control purposes. Zhang and Chen (2022) developed an adaptive controller based on online gravity compensation to estimate any gravity based parameters for accurate transfer of the payload from the ship. Qian, Hu, Chen, Fang, and Hu (2021) proposed an adaptive neural network based control scheme for payload transfers between two ships.

Since L&R operations at sea have traditionally been undertaken manually — little in the way of existing literature is available that addresses the dynamics and control of the entire process. The key contribution of this paper is

- to study for the first time the development of a feedback control system to automate the process of safely recovering a small vessel to a mothership
- to understand/predict the range of sea states under which this may be possible.

The only other relevant work the authors are aware of which addresses this problem, is the recent paper (Zhang, Zhao, Li, Edwards, & Belmont, 2023). In Zhang et al. (2023) the L&R problem is considered based on a relatively simple model of the mothership. These vessel dynamics are used as the basis for an MPC design. The MPC formulation in Zhang et al. (2023) relies on predicted future incoming wave profiles to predict the future response of the vessel involved in the L&R process over a moving time horizon. This requires an on-board sea wave prediction system (Al-Ani, Belmont, & Christmas, 2020) and an online real-time optimization to solve the associated MPC problem. Here a completely different control approach is adopted. In this paper a more complex model of the mothership response is used as the basis for developing (off-line) a parameter varying feedback gain synthesized from adopting a 'robust control' paradigm (specifically in this case, a sliding mode approach). The resulting controller is much less computationally intensive to implement and does not require a sea wave prediction system. The approach adopted in this paper therefore has potentially significant benefits in terms of retrofitability and financial cost.

The control approach used in this paper is separated into control of the crane cable length and control of the boom position, and hence the suspension point. These two problems are addressed independently. SMC has been used for length control and an Integral Sliding Mode Control (ISMC) approach is used for the control of the lateral movement of the boom. This approach has been adopted because of its strong robustness properties which have been widely studied and well documented (Shtessel, Edwards, Fridman, & Levant, 2014). To deal with disturbances and the absence of robustness during the reaching phase traditionally associated with SMC, integral sliding mode control has been implemented for the control of many types of underactuated systems like the flexible joint robot (Alam et al., 2018; Khan et al., 2022), cart–pole system (Chawla, Chopra, & Singla, 2021) and a 4DOF tower crane (Zhang, Zhang, & Cheng, 2019). Modelling of the L&R system involves a modular approach consisting of wave motion effects, ship motion estimation, crane/small vessel modelling (and the control algorithm). In particular, the wave motion and ship motion prediction models will both possess inaccuracies when compared to the real situation. Thus, it is essential to employ a robust control approach which can deal effectively with modelled and unmodelled

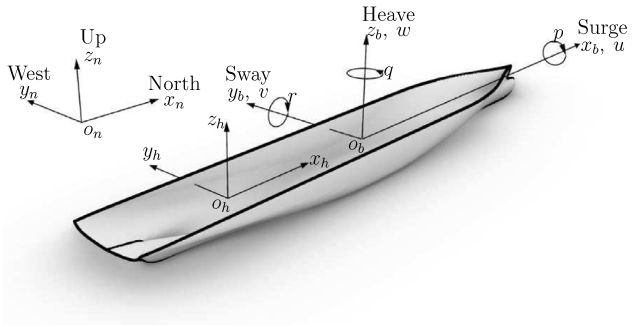

Fig. 3. The six degrees of freedom and different coordinate systems for the ship (Perez, 2006).

system uncertainties. This paper is structured as follows. In Sections 2 and 3 the mathematical models of the mothership and the crane are described respectively, in Section 4 the novel control architecture is developed and in Section 5 some simulation results are shown. An attempt is made to understand the range of sea states in which using this approach is feasible. Some concluding remarks are provided at the end of the paper.

2. Ship motion modelling

This section describes the simulation environment which has been developed to test the control algorithms proposed for L&R. High-fidelity models of the sea can be obtained from Computational Fluid Dynamics (CFD) methods like Large Eddy Simulations (LES), Direct Numerical Simulations (DNS) and Reynolds Averaged Navier–Stokes (RANS) equations. They are also able to provide accurate estimates of fluid–structure interactions between the vessels and the sea (Perez, 2006). However, these methods are extremely time consuming and computationally intensive processes, and thus unsuitable for our purpose. Here a unified seakeeping-manoeuvring model, which is used in advanced ship motion simulators that operate in the time domain (Perez, 2006), is used to model the mothership motions. The sea environment and the ship model is based on Perez (2006). In conjunction with their highly cited book (Perez, 2006), the authors created a SIMULINK based Marine Systems Simulator (MSS) (Fossen & Perez, 2004). This simulation package has been used to generate ship motions under various sea conditions. The underlying mothership simulation is based on a unified state-space model. This has many advantages over the simpler motion superposition models. In particular it includes the radiation forces during manoeuvring with greater accuracy, as it considers the radiation forces produced due to control action, along with those produced by the waves.

To integrate the motion of a ship with the on-board crane model which will be discussed in the sequel, the following reference frames are needed (see Fig. 3) as described in (Perez, 2006):

- The n-frame is centred about a fixed point on the earth.
- The b-frame is centred about a fixed point on the ship's hull and coincides with the principal axes of rotation.
- The h-frame is centred relative to the time-averaged response of the ship. The plane x_h, y_h coincides with the average water level, x_h points in the average yaw direction and $x_h = y_h = 0$ at the average centre of gravity.

For marine operations, the surface of the sea is broadly classified into sea states as shown in Table 1. This classification is made on the basis of the significant height ($H_{1/3}$) of the waves, which refers to the mean wave height of the highest one-third of the waves.

Table 1
Sea state description (Perez, 2006).

Sea state	$H_{1/3}$ range (m)	Sea description
0	0	Calm (glassy)
1	0–0.1	Calm (rippled)
2	0.1–0.5	Smooth (wavelets)
3	0.5–1.25	Slight
4	1.25–2.5	Moderate
5	1.25–4	Rough
6	4–6	Very rough
7	6–9	High
8	9–14	Very high
9	>14	Phenomenal

3. 2D adjustable boom model

This section focuses on the development of a two-dimensional model of a crane with an adjustable boom, and its interaction with the small vessel to be recovered. Many rigid body models of crane systems exist in the literature, but in this paper, a particular form of boom crane and its interaction with the ship model will be described from first principles. This model will then be considerably simplified to obtain a 'control oriented' model which will be used for the design of the control system. In the literature, crane modelling can be broadly categorized into attempts to create either distributed-mass or lumped-mass models (Abdel-Rahman, Nayfeh, & Masoud, 2003). In the distributed-mass model, the crane hoist cable is modelled as a distributed-mass system. The hook and small vessel are combined to form a point mass and act as boundary conditions for the distributed-mass hoisting cable. This model is valid when the lumped mass is of the same order of magnitude as the mass of the cable. As expected, this has very limited applications. The lumped-mass model is the more common and practical modelling method. In this section the hoisting cable is considered massless, with the hook and small vessel being lumped together to form a point mass.

The most widely utilized method for crane modelling is the Euler–Lagrange approach. This method is based on the conservation of energy and has been widely used by Nayfeh, Ragab, and Al-Maaitah (2002), Abdel-Rahman et al. (2003), Chin, Nayfeh, and Abdel-Rahman (2001), Chin et al. (2000), Wen, Homaifar, Bikdash, and Kimiaghalam (1999), Tuan, Lee, Nho, and Cuong (2015) to obtain the equations of motion of the crane's payload. An advantage of this method is that the generalized variables can be selected and specified as per requirement.

A two-dimensional model of the mothership and crane is considered in this paper with the consideration of roll, sway and heave motions. These motions have been considered out of the six degrees of freedom available due to their prominent impact on the L&R process. Excessive movements in any of these degrees of freedom can lead to possible collision of the small vessel with the hull of the mothership, and in worst case scenarios, lead to the capsizing of the small vessel. The 2D crane model consists of a tower fixed on the mothership, with a boom at a right angle to this tower. The boom is long enough to have its end extending past the hull of the mothership. The hook is attached to the end of the boom (suspension point) using a cable connected to the winch. Finally, the hook is attached to the small vessel being lifted from the sea (or lowered into the water). A key feature of this model is that the suspension point is movable - i.e. the boom length is not fixed. This flexibility will be exploited to introduce an additional control input to the system.

The small vessel is represented by the solid blue circle in Fig. 4, i.e. effectively as a point mass. The mothership, denoted by the blue rectangle, is moving in the outward perpendicular direction from the y_b, z_b-plane. All of the additional nomenclature used to describe the crane is presented in Table 2.

The green line perpendicular to the hull represents the crane tower and the other green line represents the boom. The blue line depicts the crane cable connecting the boom suspension point to the small vessel, which is the payload here. The small vessel is considered a point mass in this model.

The following abbreviations will be used for the remainder of the developments: $S_\phi = \sin\phi$, $C_\phi = \cos\phi$, $S_{\phi-\alpha} = \sin(\phi-\alpha)$ etc. This simplifies notationally the developments which follow.

From Fig. 4, the position vector of the small vessel in the n-frame, P_l, can be computed as

$$P_l = \begin{bmatrix} dC_\phi + lS_\alpha - hS_\phi + \eta_2 \\ dS_\phi - lC_\alpha + hC_\phi + \eta_3 \end{bmatrix} \tag{1}$$

where η_2 and η_3 denote the ship's displacement (m) in the y_n and z_n directions from the origin of the b-frame to the origin of the n-frame. Both components of P_l are measured in metres. Note that here it is assumed the yaw angle of the mothership, $\psi \approx 0$ and the crane is positioned at $x_b = 0$. It is also assumed that the boom can be adjusted thus altering the point of suspension. This means that the quantity d is not a constant but a function of time, and this results in an inertial effect caused by the boom. Here the boom is modelled as a beam. For preliminary calculations, it has been modelled as a point mass located at the centre of the boom. The position vector of this point in the b-frame is

$$P_{boom} = \begin{bmatrix} d - \frac{a}{2} \\ h \end{bmatrix} \tag{2}$$

where, a is the constant boom length, which can only move parallel to the y_b axis.

Applying a coordinate transformation to get its position in the n-frame yields

$$P_a = \begin{bmatrix} C_\phi & -S_\phi \\ S_\phi & C_\phi \end{bmatrix} P_{boom} + \begin{bmatrix} \eta_2 \\ \eta_3 \end{bmatrix} = \begin{bmatrix} dC_\phi - \frac{aC_\phi}{2} - hS_\phi + \eta_2 \\ dS_\phi - \frac{aS_\phi}{2} + hC_\phi + \eta_3 \end{bmatrix} \tag{3}$$

Both components of P_{boom} and P_a are measure in metres. An Euler–Lagrange approach will now be adopted to develop a model of this system. The complete development of the governing equations of motion in each generalized coordinate is given in Appendix. Exploiting Eqs. (A.11d), (A.12d) and (A.13d) in the generic form of Eq. (A.7) results in the dynamical 2D model of the system which can be written as

$$\begin{bmatrix} m & 0 & -mS_{\phi-\alpha} \\ 0 & ml^2 & mlC_{\phi-\alpha} \\ -mS_{\phi-\alpha} & mlC_{\phi-\alpha} & m+M \end{bmatrix} \begin{bmatrix} \ddot{l} \\ \ddot{\alpha} \\ \ddot{d} \end{bmatrix} + \underbrace{\begin{bmatrix} f_l(q,\dot{q}) \\ f_\alpha(q,\dot{q}) \\ f_d(q,\dot{q}) \end{bmatrix}}_{f(q,\dot{q})} + \underbrace{\begin{bmatrix} \varsigma_l \\ \varsigma_\alpha \\ \varsigma_d \end{bmatrix}}_{\varsigma} = \begin{bmatrix} \tau_l \\ 0 \\ \tau_d \end{bmatrix} \tag{4}$$

where the internal forces $f(q,\dot{q})$ are

$$f_l(q,\dot{q}) = m\left(-l\dot{\alpha}^2 - gC_\alpha\right) \tag{5a}$$

$$f_\alpha(q,\dot{q}) = ml\left(2\dot{l}\dot{\alpha} + gS_\alpha\right) \tag{5b}$$

$$f_d(q,\dot{q}) = m\left(2\dot{l}\dot{\alpha}C_{\phi-\alpha} + l\dot{\alpha}^2 S_{\phi-\alpha}\right) \tag{5c}$$

and the external forces ς are given componentwise by

$$\varsigma_l = m(-2d\dot{\phi}\dot{C}_{\phi-\alpha} - d\ddot{\phi}C_{\phi-\alpha} + d\dot{\phi}^2 S_{\phi-\alpha} + h\ddot{\phi}S_{\phi-\alpha} + h\dot{\phi}^2 C_{\phi-\alpha} + S_\alpha\ddot{\eta}_2 - C_\alpha\ddot{\eta}_3) \tag{6a}$$

$$\varsigma_\alpha = ml(-2\dot{d}\dot{\phi}S_{\phi-\alpha} - d\ddot{\phi}S_{\phi-\alpha} - d\dot{\phi}^2 C_{\phi-\alpha} - h\ddot{\phi}C_{\phi-\alpha} + h\dot{\phi}^2 S_{\phi-\alpha} + C_\alpha\ddot{\eta}_2 + S_\alpha\ddot{\eta}_3) \tag{6b}$$

$$\varsigma_d = (m+M)(-h\ddot{\phi} + C_\phi\ddot{\eta}_2 + S_\phi\ddot{\eta}_3 - d\dot{\phi}^2 + gS_\phi) + Ma\dot{\phi}^2/2 \tag{6c}$$

Note that in this paper it is assumed that q, ϕ, η_2, η_3, and their derivatives, are known and therefore $f(q,\dot{q})$ and ς are available for control design.

4. Control design

In this section two controllers are proposed for the non-linear model in (4). The first controller is a higher-order sliding mode one which is

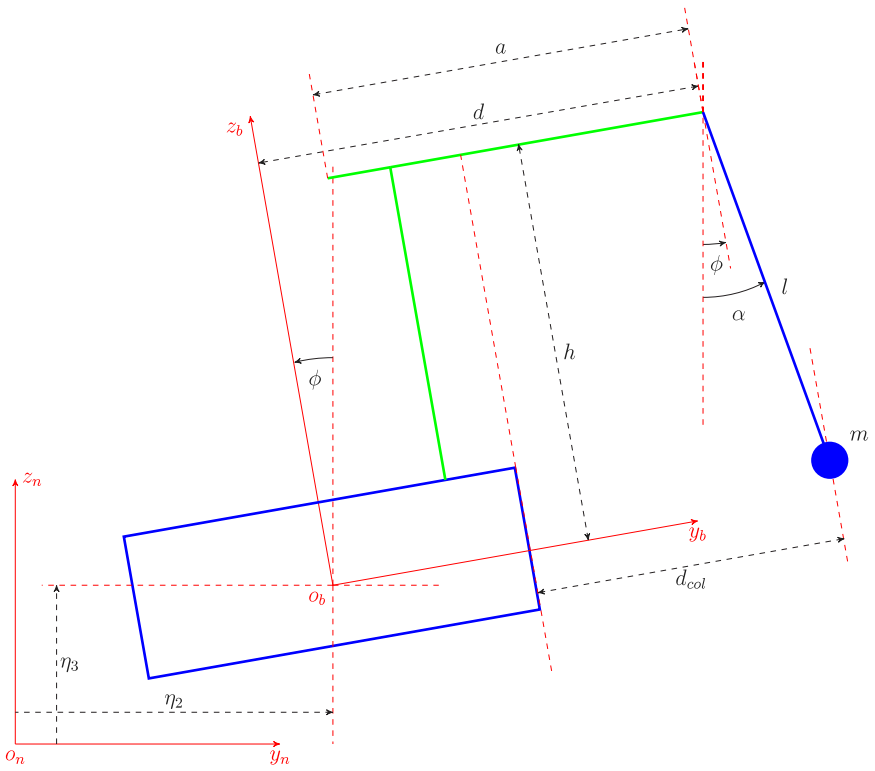

Fig. 4. 2D model of the mothership and small vessel.

Table 2
Ship model nomenclature.

a	Fixed length of the boom (m)
d	Perpendicular distance between the suspension point and z_b axis (m)
d_0	Perpendicular distance between the suspension point and mothership's hull (m)
d_{col}	Perpendicular distance between the centre of the small vessel and mothership's hull (m)
h	Perpendicular distance between the boom and y_b axis (m)
l	Length of hoisting cable from the suspension point to the small vessel (m)
m	Mass of the small vessel (kg)
M	Mass of the boom (kg)
α	Angle made by the hoisting cable with the z_n axis (rad)

tasked with controlling the cable length l through τ_l, whilst the second controller is tasked with minimizing the (oscillatory) motion of the small vessel when suspended. These two control objectives are treated as decoupled for the purposes of design.

4.1. Length control

For the purposes of control design, the dynamics for the cable length l in (4) can be expressed as

$$\ddot{l} = S_{\phi-\alpha}\ddot{d} - \frac{f_l + \varsigma_l - \tau_l}{m} + \mu_l \tag{7}$$

where μ_l represents an unknown, but bounded, uncertainty capturing plant/model mismatch. In this paper the control law for τ_l is chosen to have the following structure

$$\tau_l = m(\tau_l^n + \tau_l^f + \tau_l^{smc}) \tag{8}$$

where τ_l^n is a non-linear feedback term, τ_l^f is a feed-forward term depending on the demanded length profile, and τ_l^{smc} is a term to induce a second-order sliding motion (Levant, 2005). Substituting (8) into (7) yields

$$\ddot{l} = S_{\phi-\alpha}\ddot{d} - \frac{f_l + \varsigma_l}{m} + \tau_l^n + \tau_l^f + \tau_l^{smc} + \mu_l \tag{9}$$

then selecting τ_l^n as

$$\tau_l^n = -S_{\phi-\alpha}\ddot{d} + \frac{f_l + \varsigma_l}{m} \tag{10}$$

and substituting into (9) yields

$$\ddot{l} = \tau_l^f + \tau_l^{smc} + \mu_l \tag{11}$$

Note that the term τ_l^n in (10) essentially decouples the dynamics associated with the cable shown in (7) from the other two second order systems which make up the overall system in (4). This requires knowledge of the ship states — but these would be readily available on modern vessels. Any mismatches (for example inaccuracies in measurement) would need to be absorbed into the term μ_l in (11) capturing the lumped mass model uncertainty. Define the sliding surface, σ_l, as

$$\sigma_l = l - l_0 \tag{12}$$

where l_0 is the reference length, then it follows from (11) that

$$\ddot{\sigma}_l = \ddot{l} - \ddot{l}_0 = \tau_l^f + \tau_l^{smc} + \mu_l - \ddot{l}_0 \tag{13}$$

which, by selecting

$$\tau_l^f = \ddot{l}_0 \tag{14}$$

reduces to

$$\ddot{\sigma}_l = \tau_l^{smc} + \mu_l \tag{15}$$

Since the uncertainty μ_l appears in the second derivative of σ_l, the robustness term τ_l^{smc} must be chosen as a second-order SMC to force $\sigma_l = \dot{\sigma}_l = 0$ and subsequently ensure $l \to l_0$ despite the uncertainty. Robust finite time convergence of both σ and $\dot{\sigma}$ to zero in (15) was studied in Levant (2005). Here τ_l^{smc} is chosen as the following quasi-continuous SMC (Levant, 2005) structure

$$\tau_l^{smc} = -\rho_l \frac{\dot{\sigma}_l + |\sigma_l|^{\frac{1}{2}} sign(\sigma_l)}{|\dot{\sigma}_l| + |\sigma_l|^{\frac{1}{2}}} \tag{16}$$

Remark. The controller for length regulation given in (8) where the components τ_l^n, τ_l^f and τ_l^{smc} are in turn given in (10), (14) and (16) respectively, has only the gain ρ_l, which forms part of (16), as design freedom. This makes tuning straightforward. As proved in Levant (2005), if the gain ρ_l is chosen sufficiently large enough with respect to the magnitude of μ_l, then $\sigma_l \to 0$ and $\dot{\sigma}_l \to 0$ in a finite time.

4.2. Collision distance control

In this section a control law is designed for τ_d which aims to maintain a specific distance between the mothership and the small vessel. This distance is referred to as the collision distance d_{col} and is defined such that $d_{col} < 0$ indicates a collision has occurred. Since l is being controlled independently through τ_l, it is assumed for the purposes of control design that the effects of $\dot{l}$ (m/s) and $\ddot{l}$ (m/s^2) can be ignored, this reduces the Euler–Lagrange model in (4) to

$$\underbrace{\begin{bmatrix} ml^2 & mlC_{\phi-\alpha} \\ mlC_{\phi-\alpha} & m+M \end{bmatrix}}_{\tilde{M}(\tilde{q})} \ddot{\tilde{q}} + \underbrace{\begin{bmatrix} \tilde{f}_\alpha(\tilde{q},\dot{\tilde{q}}) \\ \tilde{f}_d(\tilde{q},\dot{\tilde{q}}) \end{bmatrix}}_{\tilde{f}(\tilde{q},\dot{\tilde{q}})} + \underbrace{\begin{bmatrix} \varsigma_\alpha \\ \varsigma_d \end{bmatrix}}_{\tilde{\varsigma}} = \underbrace{\begin{bmatrix} 0 \\ \tau_d \end{bmatrix}}_{\tilde{\tau}} \tag{17}$$

where the new generalized coordinates are given by $\tilde{q} = \begin{bmatrix} \alpha & d \end{bmatrix}^T$, and the simplified internal forces are given by

$$\tilde{f}_\alpha(\tilde{q},\dot{\tilde{q}}) = mlgS_\alpha \tag{18}$$

$$\tilde{f}_d(\tilde{q},\dot{\tilde{q}}) = ml\dot{\alpha}^2 S_{\phi-\alpha} \tag{19}$$

Solving (17) for $\ddot{\tilde{q}}$ yields

$$\ddot{\tilde{q}} = \tilde{M}(\tilde{q})^{-1}\left(\tilde{\tau} - \tilde{f}(\tilde{q},\dot{\tilde{q}}) - \tilde{\varsigma}\right) \tag{20}$$

and making substitutions from (17) and (18) into (20) and simplifying, using the *MATLAB Symbolic Maths Toolbox* (MATLAB, 2021), produces the following representation

$$\ddot{\alpha} = \frac{C_{\phi-\alpha}\left(mlS_{\phi-\alpha}\dot{\alpha}^2 - \tau_d + \varsigma_d\right)}{ml + Ml - mlC_{\phi-\alpha}^2} - \frac{(M+m)\left(\varsigma_\alpha + mlgS_\alpha\right)}{m^2l^2 + Mml^2 - m^2l^2C_{\phi-\alpha}^2} \tag{21}$$

$$\ddot{d} = \frac{\tau_d l - \varsigma_d l + \varsigma_\alpha C_{\phi-\alpha} - ml^2\dot{\alpha}^2 S_{\phi-\alpha} + mglS_\alpha C_{\phi-\alpha}}{l(M+m-mC_{\phi-\alpha}^2)} \tag{22}$$

In turn, (21) and (22) can be further simplified using a small angle approximation $C_{\phi-\alpha} = C_\alpha = 1$, $S_\alpha = \alpha$ and $S_{\phi-\alpha} = \phi - \alpha$, so that

$$\ddot{\alpha} = \frac{ml(\phi-\alpha)\dot{\alpha}^2 - \tau_d + \varsigma_d}{Ml} - \frac{(M+m)(\varsigma_\alpha + mlg\alpha)}{Mml^2} \tag{23}$$

$$\ddot{d} = \frac{\varsigma_\alpha + mlg\alpha}{Ml} - \frac{ml(\phi-\alpha)\dot{\alpha}^2 - \tau_d + \varsigma_d}{M} \tag{24}$$

Defining

$$\tau_d = \tilde{\tau}_d - ml(\phi-\alpha)\dot{\alpha}^2 \tag{25}$$

Eqs. (23) and (24) can be simplified to

$$\ddot{\alpha} = \frac{\varsigma_d - \tilde{\tau}_d}{Ml} - \frac{(M+m)(\varsigma_\alpha + mlg\alpha)}{Mml^2} \tag{26}$$

$$\ddot{d} = \frac{\varsigma_\alpha + mlg\alpha}{Ml} - \frac{\varsigma_d - \tilde{\tau}_d}{M} \tag{27}$$

The objective is to create a Linear Parameter-Varying (LPV) system to approximate (26)–(27) for control law design purposes: specifically

$$\underbrace{\begin{bmatrix} \delta\dot{\alpha} \\ \delta\dot{d} \\ \delta\ddot{\alpha} \\ \delta\ddot{d} \end{bmatrix}}_{\dot{x}} = \underbrace{\begin{bmatrix} 0 & 0 & 1 & 0 \\ 0 & 0 & 0 & 1 \\ -\frac{g(M+m)}{Ml} & 0 & 0 & 0 \\ \frac{mg}{M} & 0 & 0 & 0 \end{bmatrix}}_{A(l)} \underbrace{\begin{bmatrix} \delta\alpha \\ \delta d \\ \delta\dot{\alpha} \\ \delta\dot{d} \end{bmatrix}}_{x} + \underbrace{\begin{bmatrix} 0 \\ 0 \\ -\frac{1}{Ml} \\ \frac{1}{M} \end{bmatrix}}_{B(l)} \tilde{\tau}_d + \underbrace{\begin{bmatrix} 0 & 0 \\ 0 & 0 \\ -\frac{M+m}{Mml^2} & \frac{1}{Ml} \\ \frac{1}{Ml} & -\frac{1}{M} \end{bmatrix}}_{D(l)} \underbrace{\begin{bmatrix} \varsigma_\alpha + \mu_\alpha \\ \varsigma_d + \mu_d \end{bmatrix}}_{\tilde{\varsigma}} \tag{28}$$

where μ_α and μ_d represent unknown but bounded uncertainties. In (28) the states $\delta\alpha$ and δd denote perturbations of α and d from the linearization point $(0, d_0, 0, 0)$. From Fig. 4, the following geometrical relationship can be derived

$$d_{col} = d - lS_{\phi-\alpha} \tag{29}$$

assuming that $\phi \approx 0$ and using a small angle approximation

$$d_{col} \approx d + l\alpha \tag{30}$$

For the system in (28), define the coordinate transformation $x \mapsto \bar{x} = Tx$ where

$$T = \begin{bmatrix} l & 1 & 0 & 0 \\ 0 & 1 & 0 & 0 \\ 0 & 0 & 1 & 0 \\ 0 & 0 & 0 & 1 \end{bmatrix} \tag{31}$$

so that the new system state $\bar{x} = \begin{bmatrix} \delta d_{col} & \delta d & \delta\dot{\alpha} & \delta\dot{d} \end{bmatrix}^T$.

To improve low frequency performance, $\bar{x}$ can be augmented with the integral action state

$$\dot{x}_r = \begin{bmatrix} 1 & 0 & 0 & 0 \end{bmatrix} \bar{x} \tag{32}$$

such that $\tilde{x} = col(x_r, \bar{x})$. Ignoring terms related to $\dot{l}$, a linearized representation is given by

$$\dot{\tilde{x}} = \tilde{A}(l)\tilde{x} + \tilde{B}(l)\tilde{\tau}_d + \tilde{D}(l)\tilde{\varsigma} \tag{33}$$

where the system matrices are

$$\tilde{A}(l) = \begin{bmatrix} 0 & 1 & 0 & 0 & 0 \\ 0 & 0 & 0 & l & 1 \\ 0 & 0 & 0 & 0 & 1 \\ 0 & -\frac{g(M+m)}{Ml^2} & -\frac{g(M+m)}{Ml^2} & 0 & 0 \\ 0 & \frac{mg}{Ml} & -\frac{mg}{Ml} & 0 & 0 \end{bmatrix}, \quad \tilde{B}(l) = \begin{bmatrix} 0 \\ 0 \\ 0 \\ -\frac{1}{Ml} \\ \frac{1}{M} \end{bmatrix},$$

$$\tilde{D}(l) = \begin{bmatrix} 0 & 0 \\ 0 & 0 \\ 0 & 0 \\ -\frac{M+m}{Mml^2} & \frac{1}{Ml} \\ \frac{1}{Ml} & -\frac{1}{M} \end{bmatrix} \tag{34}$$

The disturbance distribution matrix $\tilde{D}(l)$ does not satisfy the matching condition (Edwards & Spurgeon, 1998) but (33) can be represented by

$$\dot{\tilde{x}} = \tilde{A}(l)\tilde{x} + \tilde{B}(l)(\tilde{\tau}_d + f_m) + \tilde{D}_u(l)f_u \tag{35}$$

where f_m and f_u respectively denote the matched and unmatched components of $\tilde{\varsigma}$ and $\tilde{D}_u$ is an appropriate distribution matrix. The representation in (35), and in particular thinking of l as a scheduling parameter, means (35) can be thought of as a Linear Parameter Varying (LPV) system.

The control scheme which will be proposed in this paper utilizes a result on scheduled control from Stilwell and Rugh (1999) which in particular involves a constructive method for finding a matrix $F(l)$ such that

$$\tilde{A}(l) + \tilde{B}(l)F(l) \tag{36}$$

is stable for all $l \in \begin{bmatrix} l_{min} & l_{max} \end{bmatrix}$ where (in this particular context) $l_{max} > l_{min} > 0$ represents the operating range of the crane. The work in Stilwell and Rugh (1999) suggests choosing

$$F(l) = \begin{cases} F_i, & l = l_i \\ \bar{F}_i(l)W^{-1}(l), & l_i < l < l_{i+1} \\ F_{i+1}, & l = l_{i+1} \end{cases} \tag{37}$$

where

$$\bar{F}_i(l) = \frac{l_{i+1} - l}{l_{i+1} - l_i}F_iW_i + \frac{l - l_i}{l_{i+1} - l_i}F_{i+1}W_{i+1} \tag{38}$$

and

$$W(l) = \begin{cases} W_i, & l = l_i \\ \frac{l_{i+1}-l}{l_{i+1}-l_i}W_i + \frac{l-l_i}{l_{i+1}-l_i}W_{i+1}, & l_i < l < l_{i+1} \\ W_{i+1}, & l = l_{i+1} \end{cases} \tag{39}$$

In the above, all the $l_i \in \begin{bmatrix} l_{min} & l_{max} \end{bmatrix}$ with $l_{i+1} > l_i$ where $l_1 = l_{min}$ and $l_{i_{max}} = l_{max}$ (i.e. they create overlapping subintervals of $\begin{bmatrix} l_{min} & l_{max} \end{bmatrix}$). The feedback gains F_i are fixed gains which stabilize the plant at the specific value of l (i.e. ensuring $\tilde{A}(l_i) + \tilde{B}(l_i)F_i$ is Hurwitz for each fixed l_i) and must satisfy the stability covering condition (Stilwell & Rugh, 1999) (i.e. there exists a feedback gain F_i which stabilizes $(\tilde{A}(l), \tilde{B}(l))$ for all fixed $l \in \begin{bmatrix} l_{min} & l_{max} \end{bmatrix}$). The positive definite matrices W_i are chosen to satisfy

$$W_i\big(A(l_i) + B(l_i)F_i\big)^T + \big(A(l_i) + B(l_i)F_i\big)W_i \leq -\kappa I \tag{40}$$

where $\kappa > 0$. In Stilwell and Rugh (1999) the choice of $F(l)$ in (37) is shown to guarantee the stability of $\tilde{A}(l) + \tilde{B}(l)F(l)$ for all $l \in \begin{bmatrix} l_{min} & l_{max} \end{bmatrix}$ provided

$$|\dot{l}| < \min_{i=1,\ldots,i_{max}-1} \frac{\kappa|l_{i+1} - l_i|}{\|W_{i+1} - W_i\|} \tag{41}$$

This choice of $F(l)$ will be used as the basis for the development of a controller for (35).

Because of the presence of uncertainty, together with the emergence of plant model mismatches resulting from the approximation used to obtain (35), a robust control methodology must be adopted. Here, a control law for $\tilde{\tau}_d$ can be designed using Integral Sliding Mode Control (ISMC) principles (Castaños & Fridman, 2006). This methodology requires a suitable choice of sliding surface, followed by an appropriate nonlinear control strategy to force the closed loop system to evolve along the surface for all time.

Firstly consider a switching function defined by

$$\sigma = G\tilde{x} - G\tilde{x}(t_0) - G\int_{t_0}^{t} \big(\tilde{A}(l) + \tilde{B}(l)F(l)\big)\tilde{x}(s)ds \tag{42}$$

where

$$G = \begin{bmatrix} 0 & 0 & 0 & 0 & M \end{bmatrix} \tag{43}$$

and $F(l)$ has been chosen so that $\tilde{A}(l) + \tilde{B}(l)F(l)$ is stable. A control law will be developed so that a sliding motion maintaining $\sigma = 0$ for all time is achieved. First it will be demonstrated that if sliding can indeed be maintained on $\sigma = 0$, then the sliding motion is given by

$$\dot{\tilde{x}} = \big(\tilde{A}(l) + \tilde{B}(l)F(l)\big)\tilde{x} + \big(I - \tilde{B}(l)G\big)\tilde{D}_u(l)f_u \tag{44}$$

To demonstrate this, differentiating (42) yields

$$\dot{\sigma} = G\dot{\tilde{x}} - G\tilde{A}(l)\tilde{x} - G\tilde{B}(l)F(l)\tilde{x} \tag{45}$$

Substituting from (35) and using the fact that $GB(l) = 1$ produces

$$\dot{\sigma} = \tilde{\tau}_d + f_m + G\tilde{D}_u(l)f_u - F(l)\tilde{x} \tag{46}$$

The equivalent control necessary to maintain sliding can be found by setting $\dot{\sigma}$ to zero and rearranging for $\tilde{\tau}_d$ (Utkin, 1992): in this specific case this yields

$$\tilde{\tau}_d^{eq} = -f_m - G\tilde{D}_u(l)f_u + F(l)\tilde{x} \tag{47}$$

Substituting $\tilde{\tau}_d^{eq}$ for $\tilde{\tau}_d$ in (35) yields the equation of motion which governs sliding as (44) as claimed.

Note that in (44) the effects of the matched uncertainty is ameliorated due to the sliding mode. The specific choice of G in (43) also ensures that $\|I - B(l)G\| \in \begin{bmatrix} 1, & \sqrt{2} \end{bmatrix}$ for $l > 1$ since

$$\|I - \tilde{B}(l)G\| = \sqrt{1 + \frac{1}{l^2}} \tag{48}$$

and so the effects of f_u are effectively managed.

Next a control law to maintain sliding will be described. Specifically consider the ISMC control law

$$\tilde{\tau}_d = F(l)\tilde{x} - \rho(\tilde{x})\frac{\sigma(t)}{\|\sigma(t)\|} \tag{49}$$

where $\rho(\tilde{x})$ is a design scalar. In (49) assuming that the uncertainties f_u and f_m remain bounded, choose $\rho(\tilde{x})$ to satisfy

$$\rho(\tilde{x}) \geq \|f_m\| + \|G\tilde{D}_u\|\|f_u\| + \varrho \tag{50}$$

where ϱ is a positive design constant.

To demonstrate that sliding is maintained, it will be shown that the so-called reachability condition

$$\sigma^T\dot{\sigma} \leq -\varrho\|\sigma\| \tag{51}$$

is satisfied (Edwards & Spurgeon, 1998).

Differentiating the expression for the switching function σ in (42) yields

$$\dot{\sigma} = G\dot{\tilde{x}} - G\tilde{A}(l)\tilde{x} - G\tilde{B}(l)F(l)\tilde{x} \tag{52}$$

By substituting for $\dot{\tilde{x}}$ from (35), and using the fact that $GB(l) = 1$, Eq. (52) simplifies to

$$\dot{\sigma} = \tilde{\tau}_d + f_m + G\tilde{D}_u(l)f_u - F(l)\tilde{x} \tag{53}$$

Then substituting for $\tilde{\tau}_d$ from (49) means

$$\dot{\sigma} = -\rho(\tilde{x})\frac{\sigma(t)}{\|\sigma(t)\|} + f_m + G\tilde{D}_u(l)f_u \tag{54}$$

It follows

$$\begin{aligned} \sigma^T\dot{\sigma} &= -\rho(\tilde{x})\|\sigma\| + \sigma^T f_m + \sigma^T G\tilde{D}_u(l)f_u \\ &\leq -\rho(\tilde{x})\|\sigma\| + \|\sigma\|\|f_m\| + \|\sigma\|\|G\tilde{D}_u(l)\|\|f_u\| \end{aligned} \tag{55}$$

If $\rho(\tilde{x})$ is chosen to satisfy (50) then from (55)

$$\sigma^T\dot{\sigma} \leq -\varrho\|\sigma\| \tag{56}$$

and so if $\sigma(0) = 0$, sliding is guaranteed to be maintained for all time (Edwards & Spurgeon, 1998).

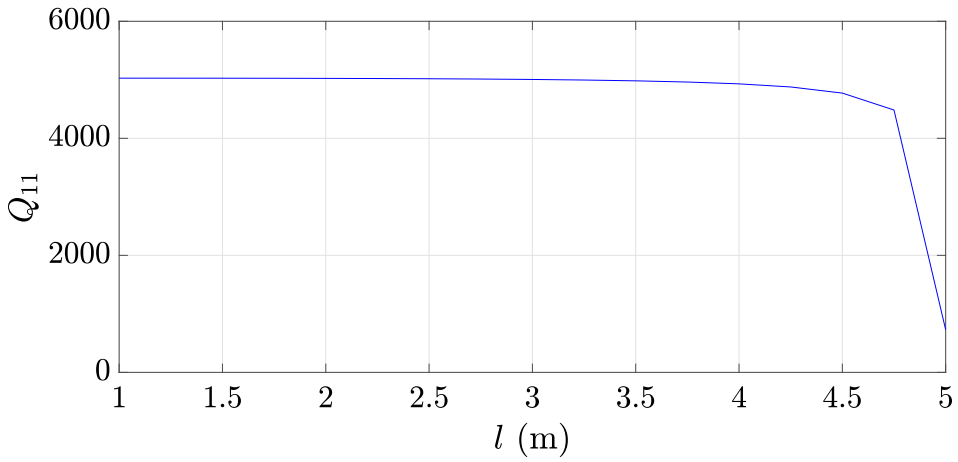

Fig. 5. Plot of $Q_{11}(l)$ with respect to l.

4.3. Design process

This subsection outlines the process for developing the control law for collision distance regulation.

1. Based on the LPV model in (28), together with the integral action component described in (32), and adopting the change of coordinates in (31), form the time varying pair $(\tilde{A}(l), \tilde{B}(l))$ as defined in (34).
2. Using the pair $(\tilde{A}(l), \tilde{B}(l))$ from Step 1 the next step involves computing the (time-varying) matrix $F(l)$ to ensure $(\tilde{A}(l) + \tilde{B}(l)F(l))$ is quadratically stable for all $l \in \begin{bmatrix} l_{min} & l_{max} \end{bmatrix}$ where l_{min} and l_{max} represent the operating range of the crane. To synthesize $F(l)$, the algorithm proposed in Stilwell and Rugh (1999) is suggested, which requires the creation of an overlapping set of intervals $\begin{bmatrix} l_i & l_{i+1} \end{bmatrix}$ with $l_{i+1} > l_i$ which must cover $\begin{bmatrix} l_{min} & l_{max} \end{bmatrix}$. The selection of the l_i's constitutes design freedom.
3. Once the l_i from Step 2 have been selected, a sequence of parameters W_i and F_i must be chosen to satisfy simultaneously the Lyapunov equations in (40) where all the matrices W_i must be positive definite and the scalar κ appearing in (40) must be positive.
4. Using the W_i and F_i synthesized in Step 3, the feedback control gain $F(l)$ can be computed as defined in Eq. (37).
5. Once $F(l)$ is chosen, all the elements of the switching function σ defined in (42) are specified since the matrix G is fixed and must be selected as given in (43).
6. The control law is given by

   $$\tilde{\tau}_d = F(l)\tilde{x} - \rho(\tilde{x})\frac{\sigma(t)}{\|\sigma(t)\|}$$

   where the modulation gain in the switching term $\rho(\tilde{x})$ must be chosen to dominate the uncertainty as specified in (50).

Note that for the purpose of implementation, the discontinuous term in (49) has been replaced by a sigmoidal approximation which removes the discontinuity which in turn removes chattering from the closed loop response (Edwards & Spurgeon, 1998).

5. Simulation results

5.1. Crane and ship modelling

In the following simulations, a ship model from the 'Marine Systems Simulator' toolbox (2021 version) (Perez, 2006) is used. The toolbox contains hydrodynamic data for a number of ships: in the following results, the S175 container ship is used as the mothership. The S175 is a large container ship with a length (between perpendiculars) of 175 m, a beam of 25.4 m, a mean draught of 9.5 m and a mass of 25×10^6 kg. The simulations were carried out in SIMULINK 2020b on a Microsoft Windows machine with 32 GB RAM and a processor speed of 4.3 GHz.

The crane model, shown in Fig. 4 has a fixed length $a = 5$ m, mass $M = 500$ kg and a height above the y_b axis $h = 7$ m. The small vessel considered is a Rigid Hull Inflatable Boat (RHIB) with a (loaded) mass $m = 1750$ kg and a beam of 1.75 m. The lifting procedure considered starts at an initial cable length $l_{max} = 5$ m, which corresponds to the waterline of the mothership, and lifts the small vessel a total of 4 m over a period of 15 s, giving a final length of $l_{min} = 1$ m. This ensures the small vessel is sufficiently clear of the deck of the mothership so that it can be brought onboard.

5.2. Control design

In (37) the feedback gains F_i were designed using a Linear Quadratic Regulator (LQR) approach, for fixed values of $l = 1.00, 1.25, \ldots, 4.75, 5.00$ m. The weighting matrices used in the control synthesis are chosen as

$$Q(l) = diag(Q_{11}(l), \quad 400, \quad 350, \quad 0, \quad 0), \qquad R = 14 \tag{57}$$

where the values of $Q_{11}(l)$ for different cable lengths are shown in Fig. 5. In $Q(l)$ the first two elements are both associated with collision distance (d_{col}) (the first entry being the integral action state) and are weighted heavily — since preventing collision is the controller's main objective. The last two entries, associated with the swing angle velocity ($\dot{\alpha}$) and suspension point velocity ($\dot{d}$), are set to zero since these are not important for achieving the main control objective. The specific choice of $Q_{11}(l)$ ensures that at the beginning of the lift (when $l = 5$ m) the controller is focused on dampening any oscillations associated with the initial conditions of the small vessel (i.e. control of the swing angle α is prioritized over d_{col}). As the lift progresses ($l < 5$ m), the priority aggressively increases to control of the collision distance.

Through the use of Linear Matrix Inequality (LMI) software (Lofberg, 2004) it can be verified that for each fixed value of l_i, and corresponding gain F_i, there is a common solution to the Lyapunov function (40) so that $W_{i+1} = W_i$ for all i. Therefore the bound in (41) becomes infinite — guaranteeing stability of (36) for any value of $\dot{l}$ within the region $l \in \begin{bmatrix} 1 & 5 \end{bmatrix}$.

In the simulations, to prevent 'chattering' (Edwards & Spurgeon, 1998), the following sigmoidal approximation of the control law $\tilde{\tau}_d$, from (49) has been used

$$\tilde{\tau}_d = F(l)\tilde{x} - \rho(\tilde{x})\frac{\sigma(t)}{\|\sigma(t)\| + \delta} \tag{58}$$

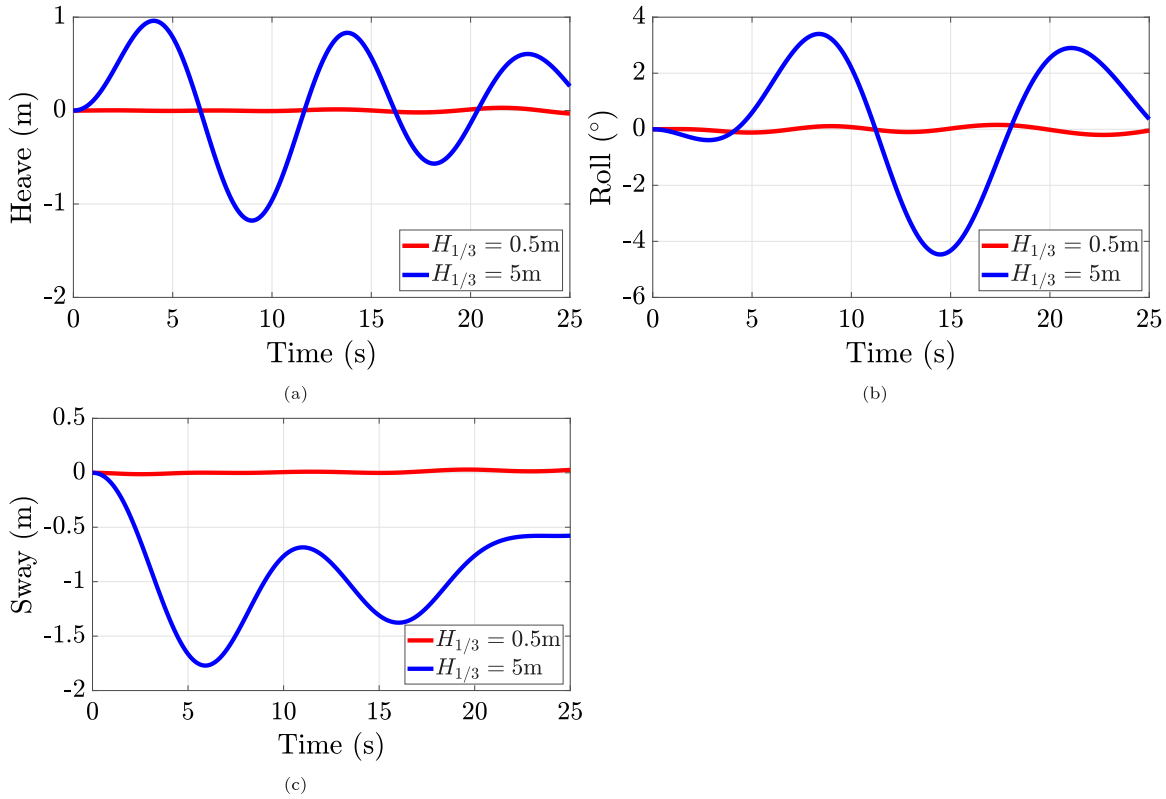

Fig. 6. Ship motion comparison for significant wave heights of $H_{1/3} = 0.5$ m and $H_{1/3} = 5$ m: (a) Heave; (b) Roll; and, (c) Sway.

where δ is a small positive design constant. In this paper $\rho(\tilde{x}) = 0.2$ and $\delta = 0.015$ has been chosen. For the second-order SMC in (16), ρ_l is chosen as 0.3 (which represents the only design parameter).

5.3. Results

5.3.1. Ship motions

The controller test scenarios are based on the motions of the S175 mothership, described in Section 5.1. During the simulations the S175 is kept at a constant speed of 10 m/s and at a constant heading of 30° (through the respective use of the engine and rudder). The sea is selected as the ITTC spectrum (Pawlowski, 2009) with a spreading factor of 2. Fig. 6 shows the responses of the S175 at two different sea states with significant wave heights $H_{1/3} = 0.5$ m (sea state 2) and $H_{1/3} = 5$ m (sea state 6). These motions have been shown here because of their relevance and use in the modelling of the crane-small vessel system. It can be seen that at sea state 6, a maximum heave displacement of under 1 m occurs and an absolute roll peak just over 4° is obtained, while the lower sea state has peak roll and heave displacements of 0.2° and 0.03 m respectively. Note that there is a 1 s period in the following simulation results where an initialization procedure takes place which aims to smooth the initial control response.

5.3.2. Crane motion for fixed boom cases

This section considers three scenarios: a low sea state condition with neutral initial conditions for the small vessel; a high sea state condition with neutral initial conditions; a high sea state condition with challenging initial conditions. Figs. 7 and 8 show the cable length (l), swing angle (α) and the suspension point's overhang ($d - w_m$) for the crane with a fixed point of suspension. Here d is the horizontal distance of the suspension point from the origin of the b-frame, defined in Fig. 4, and $w_m = 12.7$ m is equal to half the width of the mothership. The initial position of the boom is such that the suspension point is at $d = 14.2$ m. This results in an overhang distance of 1.5 m. The distance between the small vessel and the hull ($d_{col} - w_p$) along with the absolute value of the control force along the length of the cable (τ_l) are also shown in these figures. The variable d_{col} is the distance between the ship's hull and the centre of the small vessel, as defined in Fig. 4, and $w_p = 0.8$ m is equal to half the width of the small vessel. The small vessel collides with the mothership when $d_{col} - w_p = 0$ m.

As seen from Figs. 7(a) and 8(a) the length profile of the hoisting cable accurately follows the reference profile and the length control of the crane cable works as desired for all three cases. This shows the robustness of the length controller with respect to various sea states and initial conditions. The length controller is used to define a fixed trajectory for the cable length, such that the velocity of the cable before and after the recovery process is zero.

As the boom does not move, the overhang distance of the suspension point remains fixed at $d - w_m = 1.5$ m as shown in Figs. 7(b) and 8(b).

The initial condition for swing angle in Fig. 7(c) is $\alpha_0 = 0°$. For the lower sea state with $H_{1/3} = 0.5$ m, the swing angle of the cable remains low and does not exceed 1°, whereas for the higher sea state, the cable swings with an amplitude of about 4.5° after the completion of the recovery of the small vessel. When considering a non-zero initial condition for the swing angle ($\alpha_0 = -6°$) and velocity ($\dot{\alpha}_0 = -6\,°/s$) in Fig. 8(c) for the higher sea state, it is seen that the oscillations of the cable are much larger and reach an amplitude of 30° after the completion of the recovery process.

The distance between the edge of the small vessel and the hull is shown in Fig. 7(d) for the low and high sea state cases with zero initial conditions for the swing angle and angular velocity. It is seen that the small vessel does not collide with the mothership for either sea state. However, when the crane cable has an initial angular value of $\alpha_0 = -6°$ and an angular velocity of $\dot{\alpha}_0 = 6°/s$, Fig. 8(d) shows that a collision

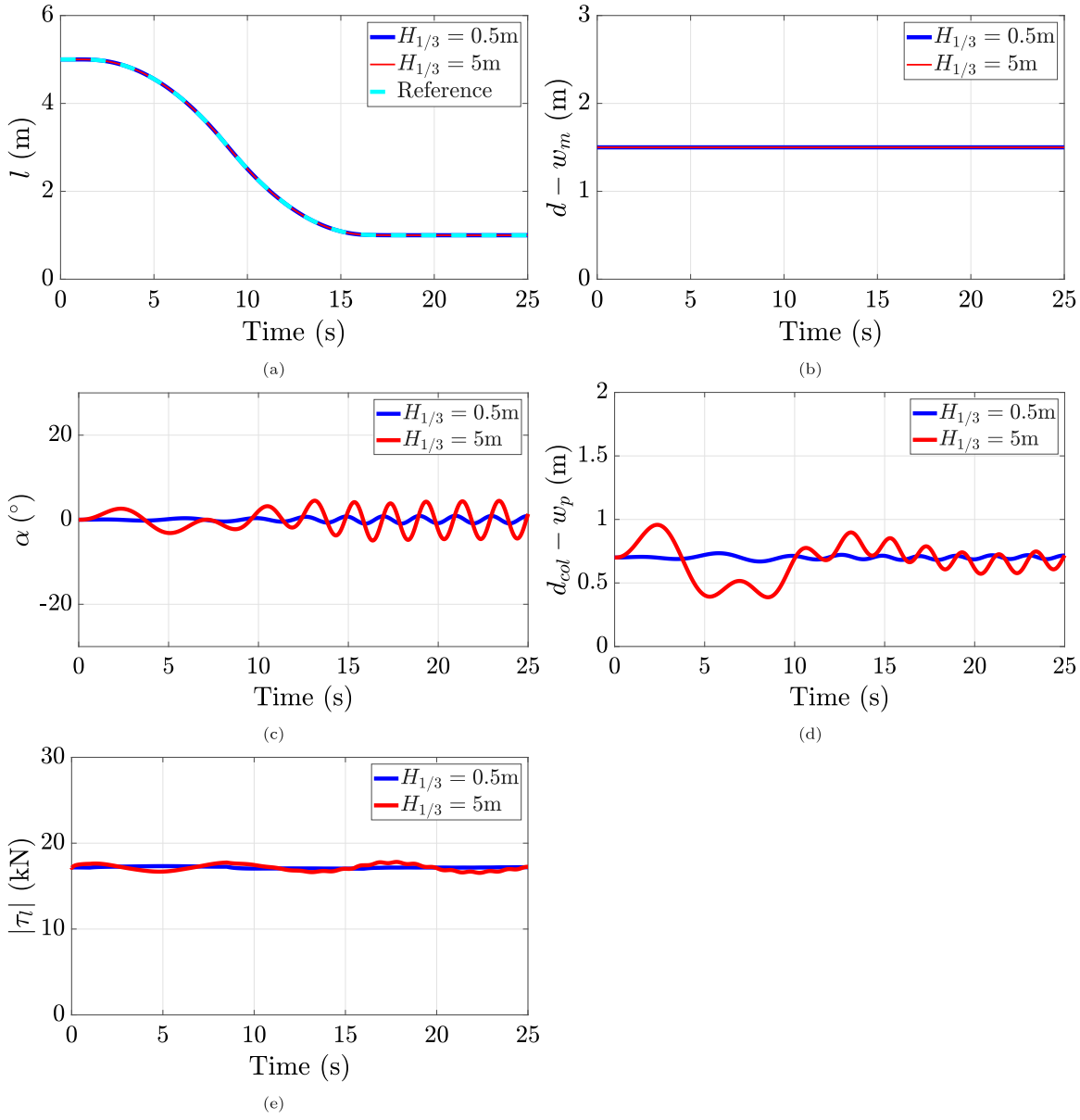

Fig. 7. Comparison of crane motions comparison with fixed boom for significant wave heights of $H_{1/3} = 0.5$ m and $H_{1/3} = 5$ m, with initial conditions $\alpha_0 = 0°$, $\dot{\alpha}_0 = 0°/s$: (a) Cable length (l); (b) Suspension point overhang ($d - w_m$); (c) Swing angle (α); (d) Separation distance ($d_{col} - w_p$); and, (e) Tension in crane cable ($|\tau_l|$).

will occur shortly before 5 s. This warrants the need for a controller to reduce the oscillations of the crane cable to prevent the collision between the mothership and the small vessel.

The absolute value of the control force on the crane cable is shown in Figs. 7(e) and 8(e). This force acts in the form of tension in the cable. For the lower sea state with zero initial conditions, the force remains consistent about 17.1 kN. This is equal to the gravitational pull on the small vessel of mass 1750 kg, which is $F = mg = 1750\,\text{kg} \times 9.81\,\text{m/s}^2 = 17.168\,\text{kN}$. At the higher sea state, it is seen that the control force is more oscillatory in nature. This can be attributed to the larger heave and roll motions in this case, which in turn have an impact on the external forces as well as the swing angle. In comparison with the higher sea state with non-zero angular initial conditions ($\alpha_0 \neq 0°$, $\dot{\alpha}_0 \neq 0\,°/s$), it is seen that while the oscillations are still centred about 17.1 kN, they are much larger in value due to the significantly higher swing angle which ranges between ±30°.

5.3.3. Crane motion for adjustable boom cases with different initial conditions

This section considers the case where the suspension point is adjustable for the same scenarios as in Section 5.3.2. Some additional 'awkward' initial conditions are also considered here. Fig. 9 displays the response of the system for the low and high sea state situations with zero initial conditions for the cable swing angle and angular velocity. The length profiles in Fig. 9(a) show that the (length) controller is robust as the cable length follows the controller-defined trajectory perfectly for both sea states.

Fig. 9(b) shows the overhang distance of the suspension point on the boom, which is adjustable, and this movement is driven by the controller output. For the lower sea state, it is seen that the crane does not show any large movement with the maximum deviation from the initial overhang distance being around 0.013 m. For the higher sea state, there is a larger change from the initial position with the maximum

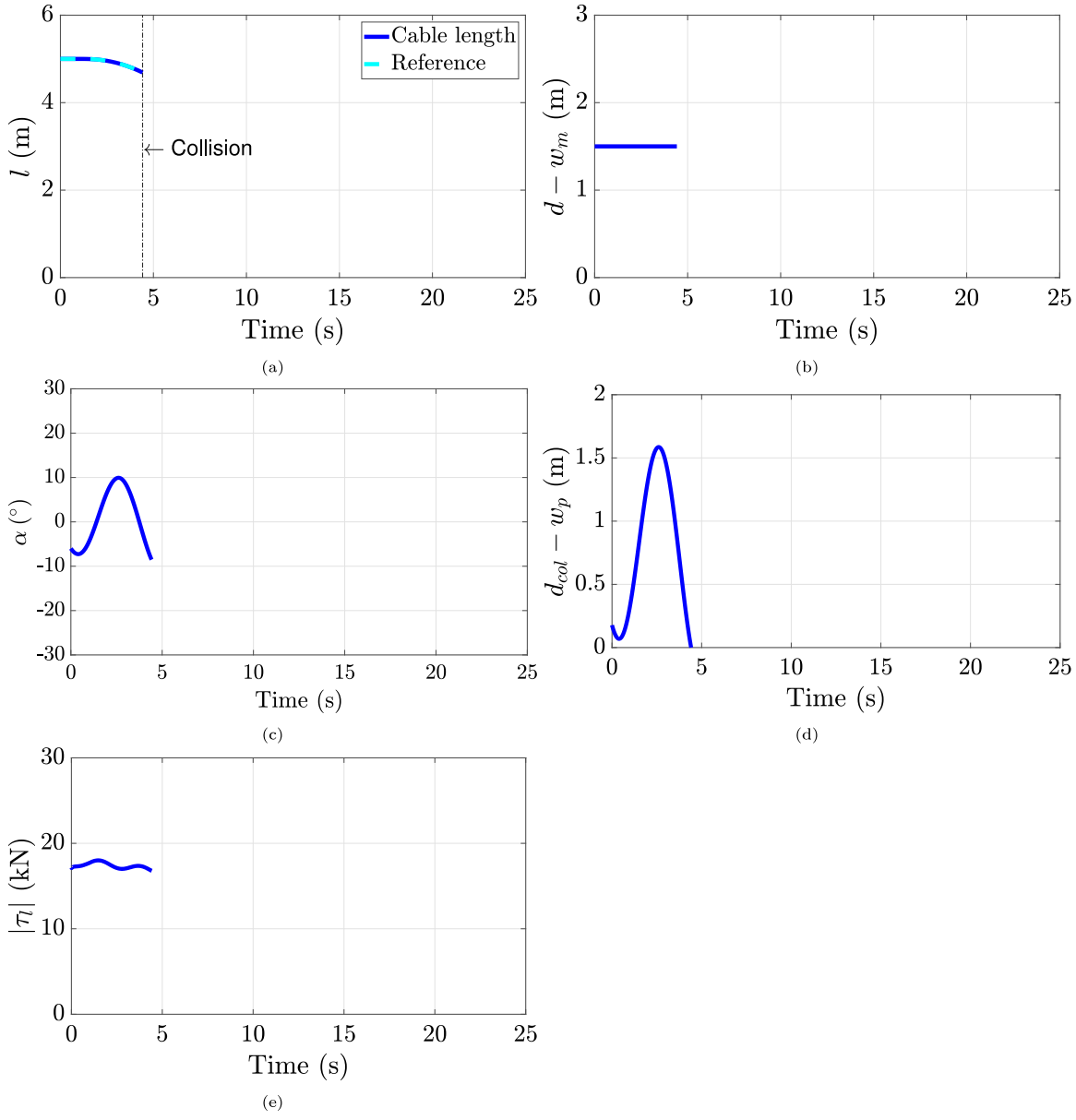

Fig. 8. Crane motions with fixed boom for a significant wave height of $H_{1/3} = 5\,\text{m}$, $\alpha_0 = -6°$ and $\dot{\alpha}_0 = -6°/\text{s}$: (a) Cable length ($l$); (b) Suspension point overhang ($d - w_m$); (c) Swing angle (α); (d) Separation distance ($d_{col} - w_p$); and, (e) Tension in crane cable ($|\tau_l|$).

value being $d - w_m = 1.77\,\text{m}$ resulting in a change of $0.27\,\text{m}$. The goal of this movement is to minimize the oscillations of the crane cable, which is represented by the swing angle (α).

The swing angle for the higher sea state is larger than that in the lower sea state as seen in Fig. 9(c). This results in the distance between the small vessel and mothership's hull deviating from the desired value of $0.7\,\text{m}$ by a greater extent. This is shown in Fig. 9(d), but it can be seen that no collision occurs in either case. The larger deviation from the desired separation distance requires a larger movement of the boom to bring the distance between the small vessel and mothership's hull to $0.7\,\text{m}$ and this is seen in the overhang distance. Due to the control action on the boom, it can be seen that the separation distance remains around $0.7\,\text{m}$ for both cases, thus demonstrating the benefit of adding a controller for the boom.

The tension in the crane cable is shown in Fig. 9(e) for the low and high sea states. It exhibits behaviour similar to that seen in the previous section for the fixed-boom cases. The lower sea state results in a consistent force of about $17.1\,\text{kN}$, while the higher sea state case shows some oscillations centred around this value due to the additional forces caused by the larger heave and roll motions, and the acceleration of the boom. The absolute values of the control forces on the boom (τ_d) are shown in Fig. 9(f). For the lower sea state, as the separation distance remains in the vicinity of the desired $0.7\,\text{m}$ value, the force on the boom is very low with a maximum value around $0.08\,\text{kN}$. For the higher sea state, the maximum force applied on the boom is around $1.8\,\text{kN}$ to counter the larger separation distance.

Figs. 10(a)–10(f) show the plots for the higher sea state with non-zero initial conditions for the swing angle and angular velocity: specifically $(\alpha_0, \dot{\alpha}_0) = \{(-6,-6), (6,-6), (-6,6), (6,6)\}$. The length profiles in all four cases follow the desired profile as seen in Fig. 10(a), once again showing the robustness of the length controller and its feasibility in operating concurrently with the boom controller under various initial conditions.

The swing angle profile in Fig. 10(c) shows a starting value of $-6°$ and an initial angular velocity of $-6°/\text{s}$. The separation distance between the small vessel and the mothership reduces from the initial

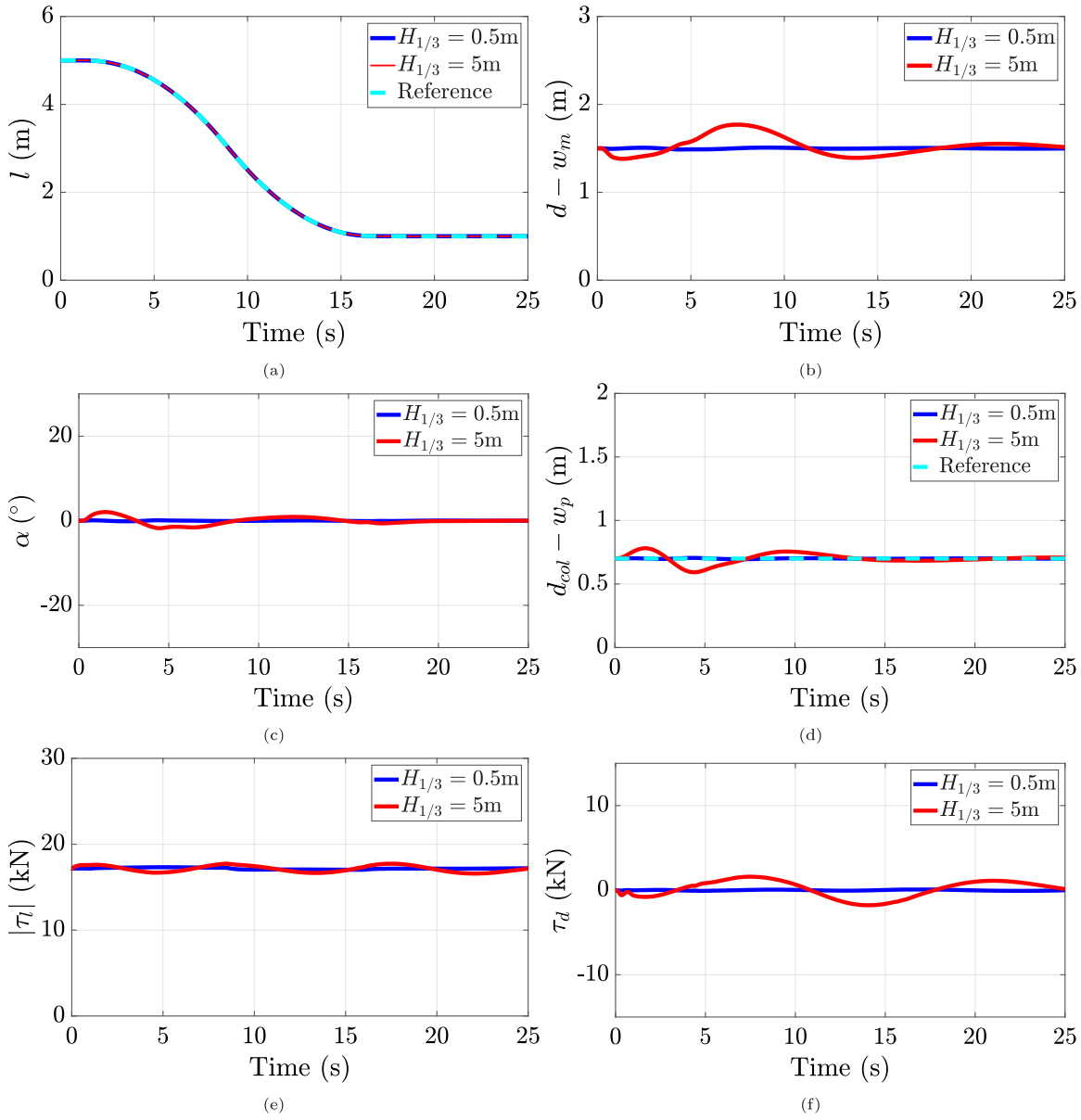

Fig. 9. Comparison of crane motions with adjustable boom for a significant wave heights of $H_{1/3} = 0.5$ m and $H_{1/3} = 5$ m, with initial conditions $\alpha_0 = 0°$ and $\dot{\alpha}_0 = 0°/s$: (a) Cable length (l); (b) Suspension point overhang ($d - w_m$); (c) Swing angle (α); (d) Separation distance ($d_{col} - w_p$); (e) Tension in crane cable ($|\tau_l|$); and, (f) Control force on boom (τ_d).

value of 0.17 m moving towards collision. The boom controller acts quickly and aggressively to bring this separation distance back to 0.7 m and hence has large initial fluctuations as seen in Fig. 10(f). The effect of this force is seen in the sharp increase in the displacement of the suspension point in Fig. 10(b). The sudden change in the acceleration of the boom also affects the control action along the length cable as seen in Fig. 10(e). As a consequence of the control action on the boom it is seen that at the end of the recovery phase of the small vessel, there is significant reduction in the swing angle.

The green line in Fig. 10(c) shows the swing angle when the initial angle is 6° and the swing angle velocity is −6°/s. This means that the position of the small vessel is such that its distance of separation from the mothership's hull is larger than the desired 0.7 m, but moves towards the mothership due to the negative angular velocity as shown in Fig. 10(d). As the small vessel is approaching the desired separation distance of 0.7 m on its own, the external control action on the boom, in Fig. 10(f), is very low in comparison to the previous case, where the controller was aggressive in nature to prevent collision and maintain the desired separation distance. The effect of this lower control force is seen on the overhang distance in Fig. 10(b), where the maximum overhang distance is less than 0.5 m from that experienced in the $(-6, -6)$ case. The effect of the lower acceleration of the boom is also seen in the less aggressive control action along the length of the cable seen in Fig. 10(e).

The red line in Fig. 10(c) covers the scenario where the initial conditions of $(\alpha_0, \dot{\alpha}_0) = (-6, 6)$, which is the polar opposite of the case considered above, which had initial conditions of $(\alpha_0, \dot{\alpha}_0) = (6, -6)$. The negative swing angle shown in Fig. 10(c) depicts that the small vessel is closer to the ship in comparison to its position at equilibrium. The positive angular velocity means that the small vessel is moving away from the mothership, thus increasing the separation distance as seen in Fig. 10(d). As in the previous case, due to the small vessel moving towards the desired separation distance of 0.7 m with its own momentum, the control force applied on the boom is not very aggressive (Fig. 10(f)). As a result of this force, the suspension point is moved by about 0.6 m in Fig. 10(b) to counter the effect of the small vessel moving away from

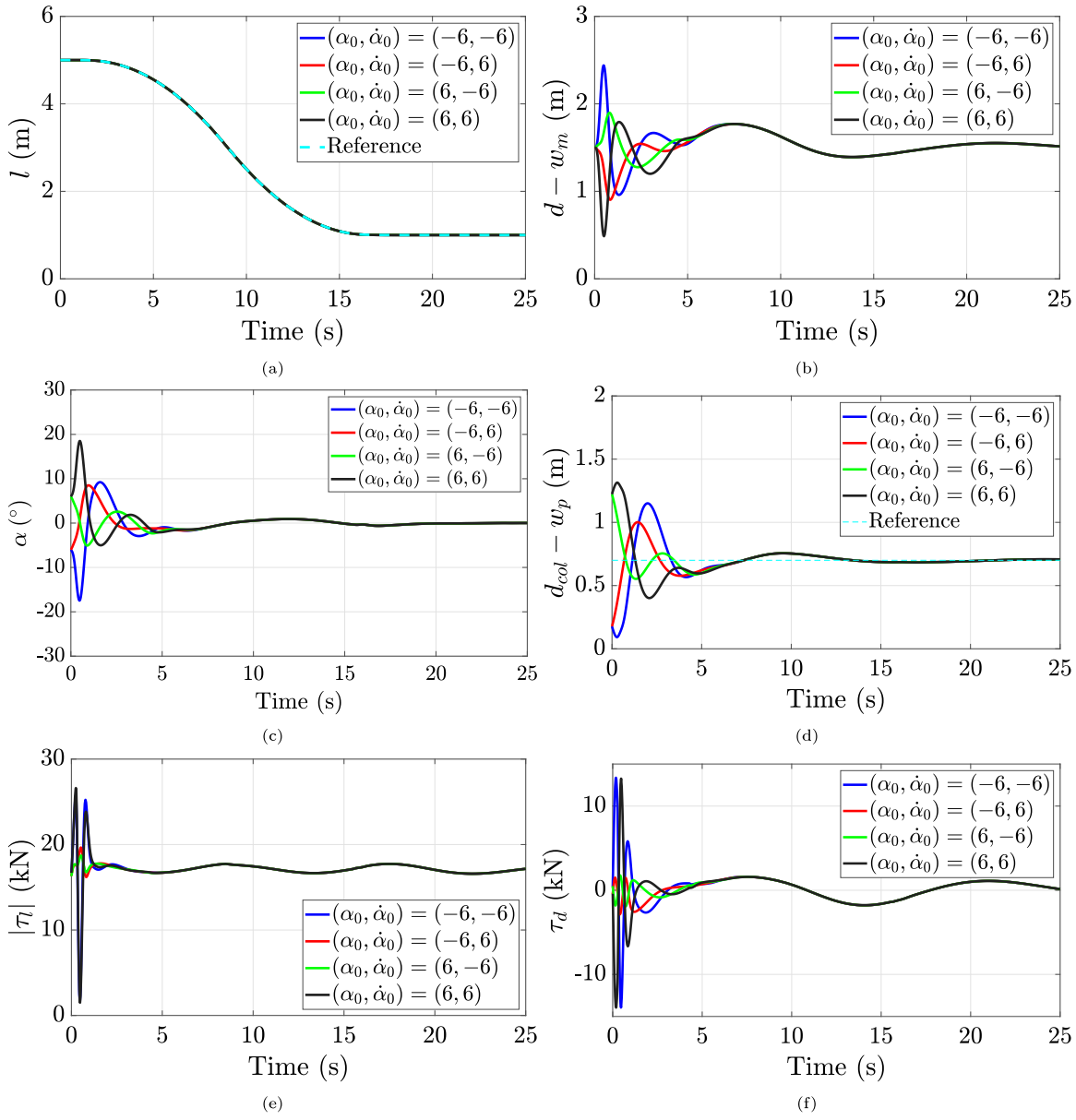

Fig. 10. Crane motions with adjustable boom for a significant wave height of $H_{1/3} = 5\,\text{m}$ and $(\alpha_0, \dot{\alpha}_0) = (\pm 6, \pm 6)$: (a) Cable length ($l$); (b) Suspension point overhang ($d - w_m$); (c) Swing angle (α); (d) Separation distance ($d_{col} - w_p$); (e) Tension in crane cable ($|\tau_l|$); and, (f) Control force on boom (τ_d).

the mothership. The low acceleration of the suspension point, in turn, has a less aggressive impact on the required tension in the cable during the recovery of the small vessel as seen in Fig. 10(e).

The final case, represented by the black lines in Figs. 10(a)–10(f), considers the initial conditions $(\alpha_0, \dot{\alpha}_0) = (6, 6)$. These values refer to a situation where the small vessel is farther from the mothership than its equilibrium position and continues to move away from it as seen in Fig. 10(c). As the small vessel is moving away from the mothership, the separation distance increases as seen in Fig. 10(d). Even though there is no threat of a collision with the mothership, this situation is treated by the controller in a manner similar to the $(-6, -6)$ case as the key variable for the boom controller is the displacement from the desired separation distance of 0.7 m. Thus, the boom controller acts aggressively, as seen in Fig. 10(f), to bring the small vessel to the desired separation distance by pulling the small vessel closer to the mothership, and then quickly moves in the opposite direction to avoid collision due to the small vessel's momentum. The effect of this control force on the suspension point is seen in Fig. 10(b), where the overhang distance reduces to 0.5 m before increasing. Fig. 10(e) shows that the sudden change in the acceleration of the boom affects the force applied by the length controller in an abrupt manner, similar to what was seen in the $(-6, -6)$ case.

The sliding surfaces for the length control and collision prevention controllers, from Eqs. (12) and (42) respectively, are shown in Fig. 11 for the four cases discussed above.

5.3.4. Minimum separation distance

This section shows the minimum separation distance for the fixed and adjustable boom cases for a range of initial conditions for the swing angle (α_0) and swing velocity ($\dot{\alpha}_0$). The range for both α_0 and $\dot{\alpha}_0$ is $[-6 : 6]$. Fig. 12 shows the worst case separation distance for the fixed-boom case under low sea state conditions. The small vessel comes within 0.1 m of the mothership's hull when the initial conditions for $(\alpha_0, \dot{\alpha}_0)$ is a subset of $\{(-6, -6), (-6, 6), (6, -6), (6, 6)\}$. The two-dimensional plot

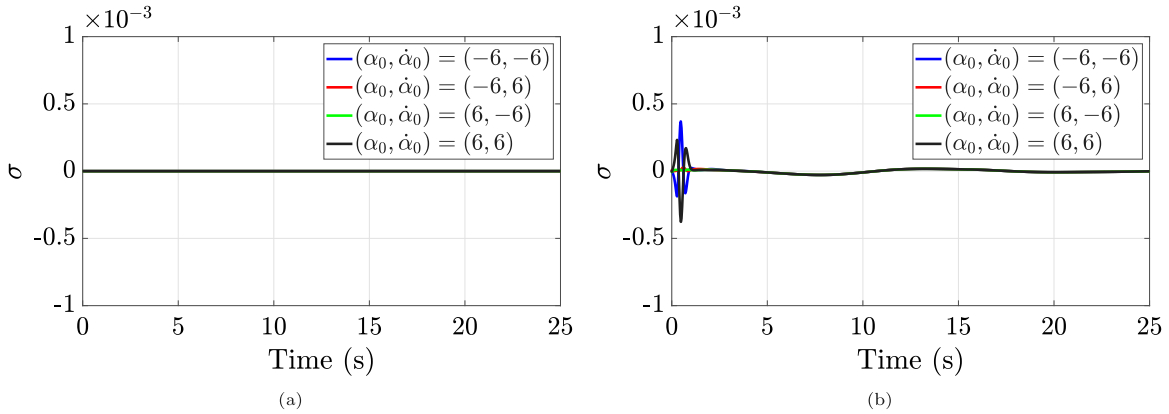

Fig. 11. Sliding surfaces for the length adjustment and collision prevention controllers. (a) Sliding surface defined in (12); (b) Sliding surface defined in (42).

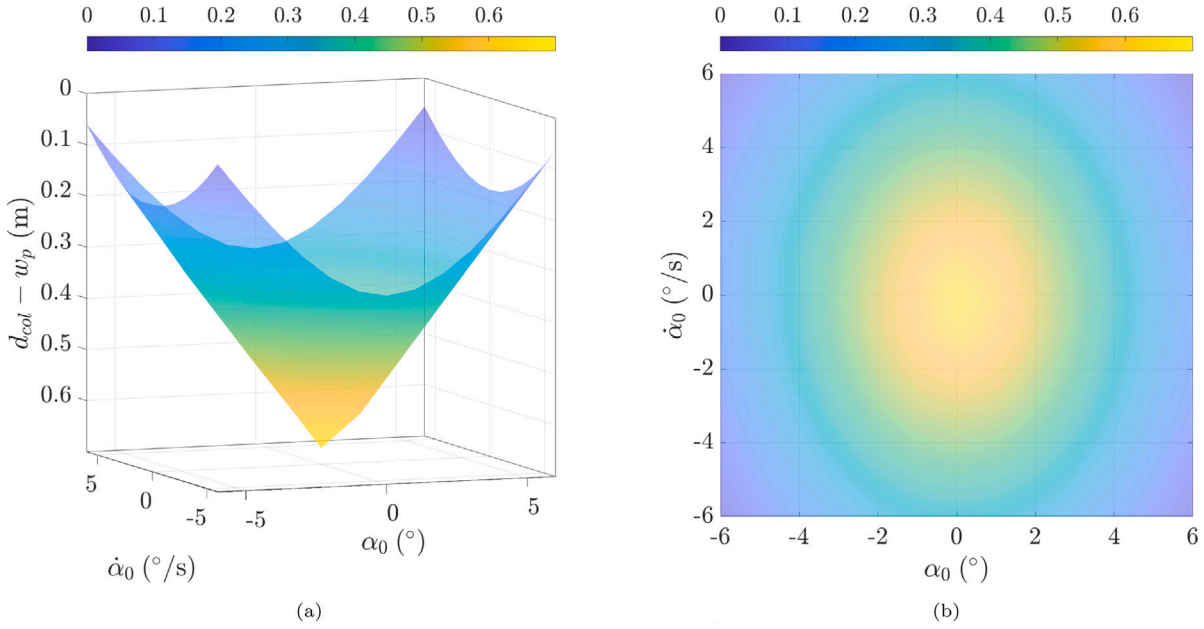

Fig. 12. Surface plots for the minimum separation distance ($d_{col} - w_p$) between the small vessel and mothership with a fixed crane boom for a range of initial swing angle (α_0) and velocities ($\dot{\alpha}_0$) for a significant wave height of $H_{1/3} = 0.5$ m: (a) 3D plot; (b) 2D plot.

in Fig. 12(b) shows symmetrical behaviour for the separation distance with the small vessel being farthest from the mothership under zero initial conditions. When the higher sea state is considered in Fig. 13, it is seen that collisions between the small vessel and the mothership will occur under various initial conditions.

The effect of the adjustable boom is seen for the lower sea state in Fig. 14. In this case the minimum separation distance is not symmetric in nature. The low separation is only seen in the cases where the initial position of the small vessel is already close to the mothership ($\alpha_0 = -6°$). However, if the position of the small vessel is away from the mothership ($\alpha_0 = 6°$), then the boom controller ensures that separation distance never reduces to the levels seen with a fixed boom. The benefit of this controller is further seen in Fig. 15 for the higher sea state situation where collision is prevented under all defined initial conditions, unlike the fixed-boom cases.

5.4. Collision analysis

The plots in Fig. 16 depict the results for various combinations of the initial swing angle (α_0) and swing angle velocities ($\dot{\alpha}_0$) at various sea states. The sea states shown here correspond to the study of the performance of the controller in sea conditions considered as rough and worse. The green sections denote the safe operation region i.e. initial conditions for which a collision free recovery can be obtained, and the red area depicts the initial conditions under which a collision occurs. The asymmetry is due to the fact that when the swing angle is negative, it implies that the small boat is initially closer to the hull of the mothership and hence more likely to collide with it. It is seen that for $\alpha_0 = (-9, -10)$, the boat is already too close to the mothership so that any movement, even with the support of the anti-collision controller, will still result in a collision. However, for $\alpha_0 = (-7, -8)$ the collision region depends on the magnitude and direction of the swing angle velocity as the collision prevention controller can negate the effect of the momentum of the payload to ensure safe operation.

It is important to note that the closest separation distance between the mothership and the small boat is experienced between $0 < t < 1$ s. During this period, the length adjustment controller is inactive. Thus the separation distance is heavily influenced by the swing angle of the cable. The magnitude of the swing angle in the direction towards the ship is the highest for the lowest sea state with $H_{1/3} = 0.5$ m for similar initial values of α and $\dot{\alpha}$. This is likely due to the control force τ_d applied on the crane boom being maximum for the lowest sea state, causing the

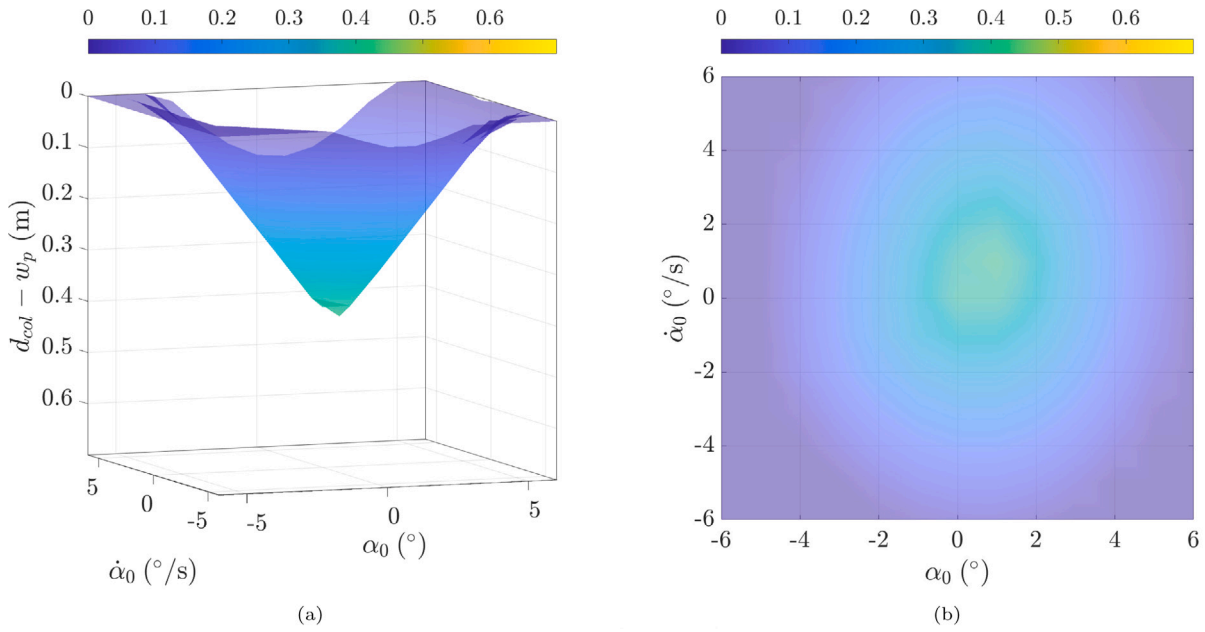

Fig. 13. Surface plots for the minimum separation distance ($d_{col} - w_p$) between the small vessel and mothership with a fixed crane boom for a range of initial swing angle (α_0) and velocities ($\dot{\alpha}_0$) for a significant wave height of $H_{1/3} = 5$ m: (a) 3D plot; (b) 2D plot.

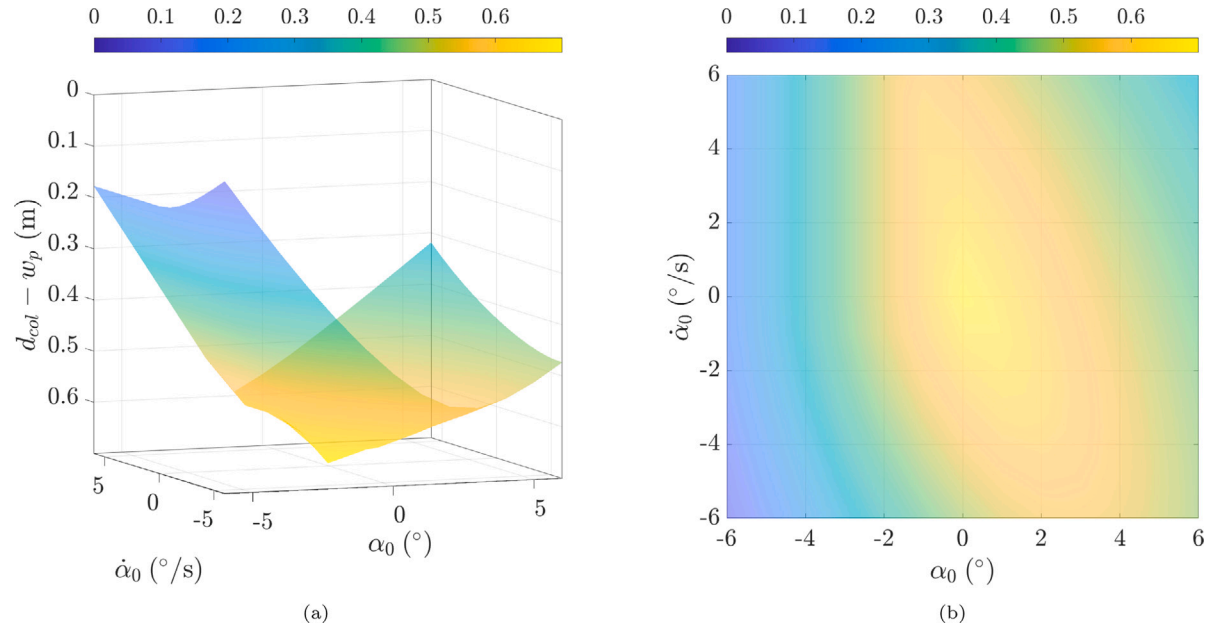

Fig. 14. Surface plots for the minimum separation distance ($d_{col} - w_p$) between the small vessel and mothership with an adjustable crane boom for a range of initial swing angle (α_0) and velocities ($\dot{\alpha}_0$) for a significant wave height of $H_{1/3} = 0.5$ m: (a) 3D plot; (b) 2D plot.

movement of the small boat in the opposite direction to be maximized. This also explains the additional point of collision for the lower sea states as seen in Fig. 16(a) at $(\alpha_0, \dot{\alpha}_0) = (-7, -7)$, while collision does not occur for the higher sea states as shown in Fig. 16(b).

6. Conclusion

This paper has proposed a control scheme for the Launch and Recovery of a small vessel to a mothership. A model has been developed for testing controllers exploiting the Marine Systems Simulator (MSS) software package, which is based on a unified seakeeping-manoeuvring model, and is used to provide the response of the mothership to the sea waves. A modified boom crane and small vessel are considered together to obtain the equations of motion governing the small vessel by utilizing the Euler–Lagrange method. Two different sea states have been considered to demonstrate the functioning of the controllers in low (sea state 3) and high (sea state 6) sea conditions. Simulations have been performed using a variety of initial conditions for the crane cable swing angle and velocity, which would be seen in real-life situations.

For the recovery of the small vessel, a single second-order sliding mode controller is used to adjust the length of the hoisting cable which is suspended from the end of the boom of the crane. Finally, an Integral Sliding Mode Controller is proposed to keep the distance between the mothership's hull and the small vessel centre at a desired value to prevent collisions, by manipulating the suspension point. The control

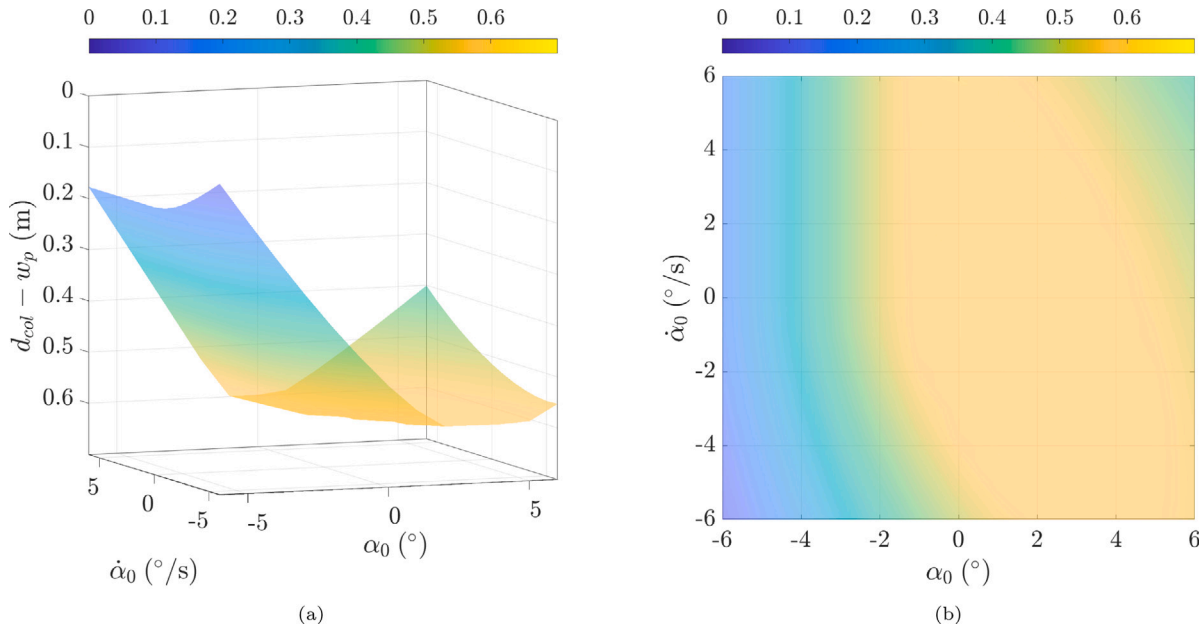

Fig. 15. Surface plots for the minimum separation distance ($d_{col} - w_p$) between the small vessel and mothership with an adjustable crane boom for a range of initial swing angle (α_0) and velocities ($\dot{\alpha}_0$) for a significant wave height of $H_{1/3} = 5$ m: (a) 3D plot; (b) 2D plot;.

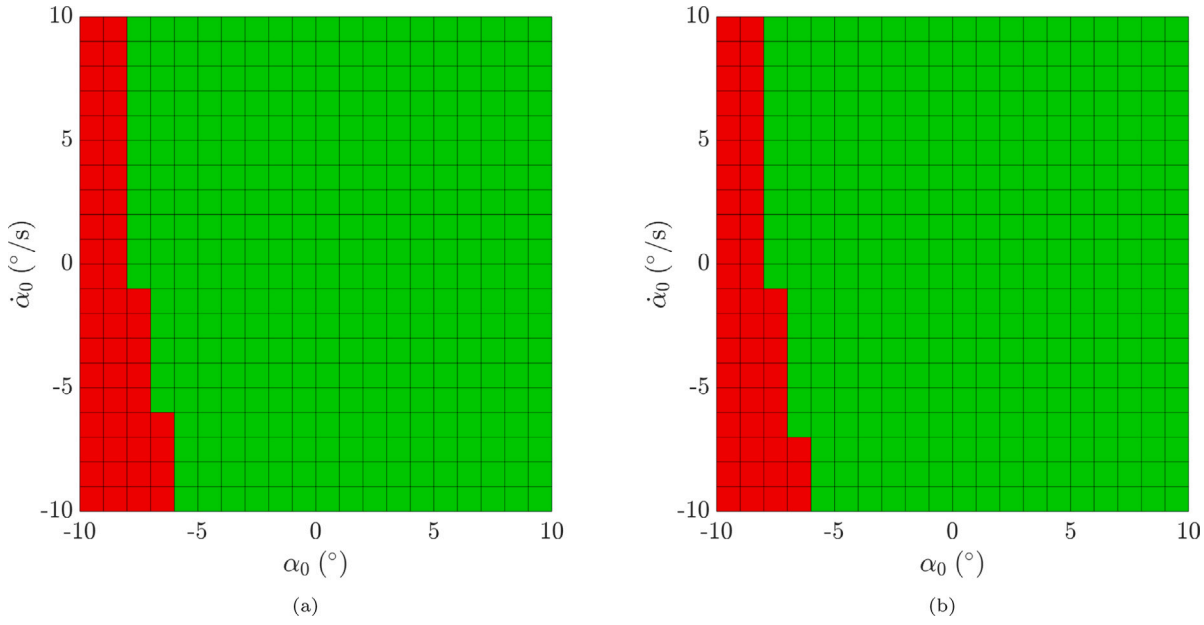

Fig. 16. Analysis of the separation distance between the mothership and small boat for a range of initial swing angle and velocities for multiple significant wave heights. The red regions indicate a collision, while the green regions indicate safe operation region. (a) $H_{1/3} = 0.5$ m, $H_{1/3} = 5$ m and $H_{1/3} = 7.5$ m; (b) $H_{1/3} = 11.5$ m and $H_{1/3} = 14$ m. (For interpretation of the references to colour in this figure legend, the reader is referred to the web version of this article.)

algorithm demonstrates its robustness by ensuring safe recovery of the small vessel in low and high sea states for various challenging initial conditions.

One of the limitations of the work presented here is that several approximations have been introduced in order to create the model used as the basis for the ISMC controller design: specifically, small angle approximations have been employed; and also terms involving the rate of change of the cable length have been ignored in order to create the LPV model. However that said, the selection of a robust ISMC controller helps in the mitigation of these issues during the control stage. Also, currently the controller requires all the states of the LPV model to be measured. This is quite a strong assumption and further work could consider the introduction of an observer system to estimate the unmeasured states. Additionally, from a purely practical perspective, the proposed method of moving the suspension point will not be possible on all existing crane systems and requires modification of existing crane setups.

Future work will focus on implementing the controller on an experimental lab-based setup to test their efficacy of the developed control algorithm. The experimental setup will include a trolley capable of

transverse motion in one direction (representing the crane boom), and a pendulum that swings parallel to this direction (representing the crane cable and the small vessel to be recovered). The whole system will be mounted on a gimbal arrangement to allow simulated mothership motion.

CRediT authorship contribution statement

Vikram Rout: Data curation, Formal analysis, Investigation, Validation, Writing – original draft. **Liam Vile:** Formal analysis, Investigation, Software, Writing – original draft. **Christopher Edwards:** Conceptualization, Formal analysis, Project administration, Supervision, Funding acquisition, Writing – review & editing. **Michael J. Belmont:** Conceptualization, Funding acquisition, Project administration, Writing – review & editing. **Guang Li:** Conceptualization, Supervision. **Dominic Taunton:** Resources, Software, Supervision, Validation, Writing – review & editing.

Declaration of competing interest

The authors declare that they have no known competing financial interests or personal relationships that could have appeared to influence the work reported in this paper.

Appendix

This appendix gives details of the development of the equations of motion of the crane system which appears in Section 3. From (2) and (3) the velocity of the small vessel and the boom is

$$\dot{P}_l = \begin{bmatrix} \dot{d}C_\phi - d\dot{\phi}S_\phi + \dot{l}S_\alpha + lC_\alpha\dot{\alpha} - h\dot{\phi}C_\phi + \dot{\eta}_2 \\ \dot{d}S_\phi + d\dot{\phi}C_\phi - \dot{l}C_\alpha + lS_\alpha\dot{\alpha} - h\dot{\phi}S_\phi + \dot{\eta}_3 \end{bmatrix} \tag{A.1}$$

and

$$\dot{P}_a = \begin{bmatrix} \dot{d}C_\phi - d\dot{\phi}S_\phi + \frac{a\dot{\phi}S_\phi}{2} - h\dot{\phi}C_\phi + \dot{\eta}_2 \\ \dot{d}S_\phi + d\dot{\phi}C_\phi - \frac{a\dot{\phi}C_\phi}{2} - h\dot{\phi}S_\phi + \dot{\eta}_3 \end{bmatrix} \tag{A.2}$$

respectively. The kinetic energy, KE (J), can be obtained from the above equations as

$$KE = \frac{1}{2}m\|\dot{P}_l\|^2 + \frac{1}{2}M\|\dot{P}_a\|^2 \tag{A.3}$$

The potential energy (J), PE_l and PE_a, of the small vessel and the boom respectively, are

$$PE_l = mgP_{l_z} = mgdS_\phi - mglC_\alpha + mghC_\phi + mg\eta_3 \tag{A.4a}$$

$$PE_a = MgP_{a_z} = MgdS_\phi - Mg\frac{aS_\phi}{2} + MghC_\phi + Mg\eta_3 \tag{A.4b}$$

where, P_{l_z} and P_{a_z} are components of the position vectors, for the small vessel and boom respectively, in the z_n direction. The total potential energy, PE (J), of the system is

$$\begin{aligned} PE &= PE_l + PE_a \\ &= mgdS_\phi - mglC_\alpha + mghC_\phi + mg\eta_3 + MgdS_\phi - Mg\frac{aS_\phi}{2} + MghC_\phi + Mg\eta_3 \end{aligned} \tag{A.5a}$$

The Lagrangian, $\mathcal{L}$ (J), of this model is

$$\mathcal{L} = KE - PE = \frac{1}{2}m\|\dot{P}_l\|^2 + \frac{1}{2}M\|\dot{P}_a\|^2 - PE_l - PE_a \tag{A.6}$$

Exploiting the Euler–Lagrange approach (Goldstein, Poole, & Safko, 2014)

$$\frac{d}{dt}\left(\frac{\partial\mathcal{L}}{\partial\dot{q}}\right) - \frac{\partial\mathcal{L}}{\partial q} = \tau \tag{A.7}$$

where the generalized coordinates have been chosen as $q = [l, \alpha, d]^T$ and $\tau = [\tau_l, 0, \tau_d]^T$ are the generalized forces. In (A.7), τ_l denotes tension (N) in the cable and τ_d denotes the force (N) applied to the boom in the y_b direction (to alter the point of suspension).

From the expressions in (A.1) and (A.2) it follows that

$$\begin{aligned} \|\dot{P}_l\|^2 = {} & \dot{l}^2 + \dot{d}^2 + \dot{\eta}_2^2 + \dot{\eta}_3^2 + d^2\dot{\phi}^2 + h^2\dot{\phi}^2 + l^2\dot{\alpha}^2 - 2h\dot{d}\dot{\phi} + 2l\dot{d}\dot{\alpha}C_{\phi-\alpha} \\ & - 2d\dot{l}\dot{\phi}C_{\phi-\alpha} - 2\dot{l}\dot{d}S_{\phi-\alpha} \\ & - 2ld\dot{\phi}\dot{\alpha}S_{\phi-\alpha} + 2h\dot{l}\dot{\phi}S_{\phi-\alpha} - 2hl\dot{\phi}\dot{\alpha}C_{\phi-\alpha} - 2h\dot{\phi}C_\phi\dot{\eta}_2 + 2l\dot{\alpha}C_\alpha\dot{\eta}_2 \\ & + 2\dot{d}C_\phi\dot{\eta}_2 + 2\dot{l}S_\alpha\dot{\eta}_2 \\ & - 2d\dot{\phi}S_\phi\dot{\eta}_2 - 2h\dot{\phi}S_\phi\dot{\eta}_3 + 2l\dot{\alpha}S_\alpha\dot{\eta}_3 + 2\dot{d}S_\phi\dot{\eta}_3 - 2\dot{l}C_\alpha\dot{\eta}_3 + 2d\dot{\phi}C_\phi\dot{\eta}_3 \end{aligned} \tag{A.8}$$

$$\begin{aligned} \|\dot{P}_a\|^2 = {} & \dot{d}^2 + d^2\dot{\phi}^2 + h^2\dot{\phi}^2 + \frac{a^2\dot{\phi}^2}{4} - ad\dot{\phi}^2 - 2h\dot{d}\dot{\phi} + \dot{\eta}_2^2 + \dot{\eta}_3^2 + 2\dot{d}C_\phi\dot{\eta}_2 \\ & - 2d\dot{\phi}S_\phi\dot{\eta}_2 + a\dot{\phi}S_\phi\dot{\eta}_2 \\ & - 2h\dot{\phi}C_\phi\dot{\eta}_2 + 2\dot{d}S_\phi\dot{\eta}_3 + 2d\dot{\phi}C_\phi\dot{\eta}_3 - a\dot{\phi}C_\phi\dot{\eta}_3 - 2h\dot{\phi}S_\phi\dot{\eta}_3 \end{aligned} \tag{A.9}$$

Substituting (A.8), (A.9), (A.4a) and (A.4b) into (A.6) yields

$$\begin{aligned} \mathcal{L} = {} & \frac{1}{2}m(\dot{l}^2 + \dot{d}^2 + \dot{\eta}_2^2 + \dot{\eta}_3^2 + d^2\dot{\phi}^2 + h^2\dot{\phi}^2 + l^2\dot{\alpha}^2 - 2h\dot{d}\dot{\phi} + 2l\dot{d}\dot{\alpha}C_{\phi-\alpha} \\ & - 2d\dot{l}\dot{\phi}C_{\phi-\alpha} - 2\dot{l}\dot{d}S_{\phi-\alpha} \\ & - 2ld\dot{\phi}\dot{\alpha}S_{\phi-\alpha} + 2h\dot{l}\dot{\phi}S_{\phi-\alpha} - 2hl\dot{\phi}\dot{\alpha}C_{\phi-\alpha} - 2h\dot{\phi}C_\phi\dot{\eta}_2 + 2l\dot{\alpha}C_\alpha\dot{\eta}_2 \\ & + 2\dot{d}C_\phi\dot{\eta}_2 + 2\dot{l}S_\alpha\dot{\eta}_2 \\ & - 2d\dot{\phi}S_\phi\dot{\eta}_2 - 2h\dot{\phi}S_\phi\dot{\eta}_3 + 2l\dot{\alpha}S_\alpha\dot{\eta}_3 + 2\dot{d}S_\phi\dot{\eta}_3 - 2\dot{l}C_\alpha\dot{\eta}_3 + 2d\dot{\phi}C_\phi\dot{\eta}_3) \\ & + \frac{1}{2}M(\dot{d}^2 + d^2\dot{\phi}^2 + h^2\dot{\phi}^2 \\ & + a\dot{\phi}S_\phi\dot{\eta}_2 + \frac{a^2\dot{\phi}^2}{4} - ad\dot{\phi}^2 - 2h\dot{d}\dot{\phi} + \dot{\eta}_2^2 + \dot{\eta}_3^2 + 2\dot{d}C_\phi\dot{\eta}_2 - 2d\dot{\phi}S_\phi\dot{\eta}_2 \\ & - 2h\dot{\phi}C_\phi\dot{\eta}_2 + 2\dot{d}S_\phi\dot{\eta}_3 \\ & + 2d\dot{\phi}C_\phi\dot{\eta}_3 - a\dot{\phi}C_\phi\dot{\eta}_3 - 2h\dot{\phi}S_\phi\dot{\eta}_3) + mglC_\alpha - mgdS_\phi - mghC_\phi - mg\eta_3 \\ & - MgdS_\phi \\ & + Mg\frac{aS_\phi}{2} - MghC_\phi - Mg\eta_3 \end{aligned} \tag{A.10}$$

Applying the Euler–Lagrange approach for the cable length l,

$$\begin{aligned} \frac{\partial\mathcal{L}}{\partial l} = {} & m(l\dot{\alpha}^2 + \dot{d}\dot{\alpha}C_{\phi-\alpha} - d\dot{\phi}\dot{\alpha}S_{\phi-\alpha} - h\dot{\phi}\dot{\alpha}C_{\phi-\alpha} + \dot{\alpha}C_\alpha\dot{\eta}_2 \\ & + \dot{\alpha}S_\alpha\dot{\eta}_3 + gC_\alpha) \end{aligned} \tag{A.11a}$$

$$\frac{\partial\mathcal{L}}{\partial\dot{l}} = m(\dot{l} - d\dot{\phi}C_{\phi-\alpha} - \dot{d}S_{\phi-\alpha} + h\dot{\phi}S_{\phi-\alpha} + S_\alpha\dot{\eta}_2 - C_\alpha\dot{\eta}_3) \tag{A.11b}$$

$$\begin{aligned} \frac{d}{dt}\left(\frac{\partial\mathcal{L}}{\partial\dot{l}}\right) = {} & m\,(\,\ddot{l} - \dot{d}\dot{\phi}C_{\phi-\alpha} - d\ddot{\phi}C_{\phi-\alpha} + d\dot{\phi}(\dot{\phi}-\dot{\alpha})S_{\phi-\alpha} - \ddot{d}S_{\phi-\alpha} \\ & - \dot{d}(\dot{\phi}-\dot{\alpha})C_{\phi-\alpha} \\ & + h\ddot{\phi}S_{\phi-\alpha} + h\dot{\phi}(\dot{\phi}-\dot{\alpha})C_{\phi-\alpha} + \dot{\alpha}C_\alpha\dot{\eta}_2 + S_\alpha\ddot{\eta}_2 \\ & + \dot{\alpha}S_\alpha\dot{\eta}_3 - C_\alpha\ddot{\eta}_3\,) \end{aligned} \tag{A.11c}$$

$$\begin{aligned} \frac{d}{dt}\left(\frac{\partial\mathcal{L}}{\partial\dot{l}}\right) - \frac{\partial\mathcal{L}}{\partial l} = {} & m(\ddot{l} - 2\dot{d}\dot{\phi}C_{\phi-\alpha} - d\ddot{\phi}C_{\phi-\alpha} + d\dot{\phi}^2S_{\phi-\alpha} - \ddot{d}S_{\phi-\alpha} \\ & + h\ddot{\phi}S_{\phi-\alpha} + h\dot{\phi}^2C_{\phi-\alpha} \\ & + S_\alpha\ddot{\eta}_2 - C_\alpha\ddot{\eta}_3 - l\dot{\alpha}^2 - gC_\alpha) \end{aligned} \tag{A.11d}$$

For the cable swing angle α,

$$\begin{aligned} \frac{\partial\mathcal{L}}{\partial\alpha} = {} & m(l\dot{d}\dot{\alpha}S_{\phi-\alpha} - d\dot{l}\dot{\phi}S_{\phi-\alpha} + \dot{l}\dot{d}C_{\phi-\alpha} + ld\dot{\phi}\dot{\alpha}C_{\phi-\alpha} - h\dot{l}\dot{\phi}C_{\phi-\alpha} \\ & - hl\dot{\phi}\dot{\alpha}S_{\phi-\alpha} \\ & + \dot{l}C_\alpha\dot{\eta}_2 - l\dot{\alpha}S_\alpha\dot{\eta}_2 + \dot{l}S_\alpha\dot{\eta}_3 + l\dot{\alpha}C_\alpha\dot{\eta}_3 - glS_\alpha) \end{aligned} \tag{A.12a}$$

$$\frac{\partial\mathcal{L}}{\partial\dot{\alpha}} = m\left(l^2\dot{\alpha} + l\dot{d}C_{\phi-\alpha} - ld\dot{\phi}S_{\phi-\alpha} - hl\dot{\phi}C_{\phi-\alpha} + lC_\alpha\dot{\eta}_2 + lS_\alpha\dot{\eta}_3\right) \tag{A.12b}$$

$$\begin{aligned}\frac{d}{dt}\left(\frac{\partial \mathcal{L}}{\partial \dot{\alpha}}\right) &= m\,\big(\,2l\dot{l}\dot{\alpha} + l^2\ddot{\alpha} + \dot{l}d\dot{C}_{\phi-\alpha} + l\ddot{d}C_{\phi-\alpha} - l\dot{d}(\dot{\phi}-\dot{\alpha})S_{\phi-\alpha} - \dot{l}d\dot{\phi}S_{\phi-\alpha}\\ &\quad - l\dot{d}\dot{\phi}S_{\phi-\alpha} - l\ddot{d}\dot{\phi}S_{\phi-\alpha} - l\dot{d}\dot{\phi}(\dot{\phi}-\dot{\alpha})C_{\phi-\alpha} - h\dot{l}\dot{\phi}C_{\phi-\alpha} - hl\ddot{\phi}C_{\phi-\alpha}\\ &\quad + hl\dot{\phi}(\dot{\phi}-\dot{\alpha})S_{\phi-\alpha} + \dot{l}C_\alpha\dot{\eta}_2 - l\dot{\alpha}S_\alpha\dot{\eta}_2 + lC_\alpha\ddot{\eta}_2 + \dot{l}S_\alpha\dot{\eta}_3\\ &\quad + l\dot{\alpha}C_\alpha\dot{\eta}_3 + lS_\alpha\ddot{\eta}_3\,\big) \qquad \text{(A.12c)}\end{aligned}$$

$$\begin{aligned}\frac{d}{dt}\left(\frac{\partial \mathcal{L}}{\partial \dot{\alpha}}\right) - \frac{\partial \mathcal{L}}{\partial \alpha} &= m(2l\dot{l}\dot{\alpha} + l^2\ddot{\alpha} + l\ddot{d}C_{\phi-\alpha} - 2l\dot{d}\dot{\phi}S_{\phi-\alpha} - ld\ddot{\phi}S_{\phi-\alpha}\\ &\quad - ld\dot{\phi}^2C_{\phi-\alpha} - hl\ddot{\phi}C_{\phi-\alpha}\\ &\quad + hl\dot{\phi}^2S_{\phi-\alpha} + lC_\alpha\ddot{\eta}_2 + lS_\alpha\ddot{\eta}_3 + glS_\alpha) \qquad \text{(A.12d)}\end{aligned}$$

For the boom location on the horizontal axis d,

$$\begin{aligned}\frac{\partial \mathcal{L}}{\partial d} &= m(d\dot{\phi}^2 - \dot{l}\dot{\phi}C_{\phi-\alpha} - l\dot{\phi}\dot{\alpha}S_{\phi-\alpha} - \dot{\phi}S_\phi\dot{\eta}_2 + \dot{\phi}C_\phi\dot{\eta}_3 - gS_\phi)\\ &\quad + M(d\dot{\phi}^2 - \frac{a\dot{\phi}^2}{2}\\ &\quad - \dot{\phi}S_\phi\dot{\eta}_2 + \dot{\phi}C_\phi\dot{\eta}_3 - gS_\phi) \qquad \text{(A.13a)}\\ \frac{\partial \mathcal{L}}{\partial \dot{d}} &= m(\dot{d} - h\dot{\phi} - \dot{l}S_{\phi-\alpha} + C_\phi\dot{\eta}_2 + S_\phi\dot{\eta}_3 + l\dot{\alpha}C_{\phi-\alpha}) + M(\dot{d} - h\dot{\phi}\\ &\quad + C_\phi\dot{\eta}_2 + S_\phi\dot{\eta}_3) \qquad \text{(A.13b)}\\ \frac{d}{dt}\left(\frac{\partial \mathcal{L}}{\partial \dot{d}}\right) &= m\big(\ddot{d} - h\ddot{\phi} - \ddot{l}S_{\phi-\alpha} - \dot{l}(\dot{\phi}-\dot{\alpha})C_{\phi-\alpha} - \dot{\phi}S_\phi\dot{\eta}_2 + C_\phi\ddot{\eta}_2\\ &\quad + \dot{\phi}C_\phi\dot{\eta}_3 + S_\phi\ddot{\eta}_3\\ &\quad + \dot{l}\dot{\alpha}C_{\phi-\alpha} + l\ddot{\alpha}C_{\phi-\alpha} - l\dot{\alpha}(\dot{\phi}-\dot{\alpha})S_{\phi-\alpha}\big) + M(\ddot{d} - h\ddot{\phi} + C_\phi\ddot{\eta}_2\\ &\quad - \dot{\phi}S_\phi\dot{\eta}_2 + S_\phi\ddot{\eta}_3\\ &\quad + \dot{\phi}C_\phi\dot{\eta}_3) \qquad \text{(A.13c)}\\ \frac{d}{dt}\left(\frac{\partial \mathcal{L}}{\partial \dot{d}}\right) - \frac{\partial \mathcal{L}}{\partial d} &= m(\ddot{d} - h\ddot{\phi} - \ddot{l}S_{\phi-\alpha} + 2\dot{l}\dot{\alpha}C_{\phi-\alpha} + C_\phi\ddot{\eta}_2 + S_\phi\ddot{\eta}_3 + l\ddot{\alpha}C_{\phi-\alpha}\\ &\quad + l\dot{\alpha}^2S_{\phi-\alpha}\\ &\quad - d\dot{\phi}^2 + gS_\phi) + M(\ddot{d} - h\ddot{\phi} + C_\phi\ddot{\eta}_2 + S_\phi\ddot{\eta}_3 - d\dot{\phi}^2 + \frac{a\dot{\phi}^2}{2} + gS_\phi)\\ &\qquad \text{(A.13d)}\end{aligned}$$

Using these equations in (A.7) yields the differential equations in (4).

References

Abdel-Rahman, E. M., Nayfeh, A. H., & Masoud, Z. N. (2003). Dynamics and control of cranes: A review. *Journal of Vibration and Control*, *9*(7), 863–908.

Al-Ani, M., Belmont, M., & Christmas, J. (2020). Sea trial on deterministic sea waves prediction using wave-profiling radar. *Ocean Engineering*, *207*, Article 107297.

Alam, W., Mehmood, A., Ali, K., Javaid, U., Alharbi, S., & Iqbal, J. (2018). Nonlinear control of a flexible joint robotic manipulator with experimental validation. *Strojniški Vestnik-Journal of Mechanical Engineering*, *64*(1), 47–55.

Beeston, J. (1969). Closed-loop time optimal control of a suspended load. In *Proceedings of the 4th IFAC World Congress* (pp. 39–50). Warsaw, Poland.

Bozkurt, B., & Ertogan, M. (2023). Heave and horizontal displacement and anti-sway control of payload during ship-to-ship load transfer with an offshore crane on very rough sea conditions. *Ocean Engineering*, *267*, Article 113309.

Büchel, D., & Åkerlund, N. (2015). *Development of overhead launch and recovery system* (Master's thesis).

Cao, Y., & Li, T. (2020). Review of antiswing control of shipboard cranes. *IEEE/CAA Journal of Automatica Sinica*, *7*(2), 346–354.

Castaños, F., & Fridman, L. (2006). Analysis and design of integral sliding manifolds for systems with unmatched perturbations. *IEEE Transactions on Automatic Control*, *51*, 853–858.

Chawla, I., Chopra, V., & Singla, A. (2021). Robust stabilization control of a spatial inverted pendulum using integral sliding mode controller. *International Journal of Nonlinear Sciences and Numerical Simulation*, *22*(2), 183–195.

Chen, H., & Sun, N. (2021). An output feedback approach for regulation of 5-DOF offshore cranes with ship yaw and roll perturbations. *IEEE Transactions on Industrial Electronics*, *69*(2), 1705–1716.

Chin, C., Nayfeh, A. H., & Abdel-Rahman, E. M. (2001). Nonlinear dynamics on a boom crane. *Journal of Vibration and Control*, *7*(2), 199–220.

Chin, C., Nayfeh, A. H., & Mook, D. (2000). Dynamics and control of ship mounted cranes. *Journal of Vibration and Control*, *7*(6), 891–904.

Edwards, C., & Spurgeon, S. (1998). *Sliding mode control: Theory and applications*. Taylor and Francis.

Fang, Y., Wang, P., Sun, N., & Zhang, Y. (2014). Dynamics analysis and nonlinear control of an offshore boom crane. *IEEE Transactions on Industrial Electronics*, *61*(1), 414–427.

Field, J. (1961). The optimization of the performance of an ore bridge. *Transactions of the Engineering Institute of Canada*, *5*(3), 163–169.

Fjelldal, R. (2017). Launch and recovery in an integrated, flexible and safe system (Presentation). In *Launch and recovery forum, London*.

Fossen, T., & Perez, T. (2004). Marine Systems Simulator (MSS). URL https://github.com/cybergalactic/MSS.

Goldstein, H., Poole, C., & Safko, J. (2014). *Classical mechanics* (3rd ed.). Harlow: Pearson.

Hanyok, L. W., & Smith, T. C. (2010). Launch and recovery system literature review, Technical Report, Naval Surface Warfare Center Carderock Division Bethesda MD.

Hong, K.-S., & Shah, U. H. (2019). *Dynamics and control of industrial cranes*. Springer.

Hua, M.-D., Hamel, T., Morin, P., & Samson, C. (2009). Control of a class of thrust-propelled underactuated vehicles and application to a VTOL drone. In *2009 IEEE International Conference on Robotics and Automation* (pp. 972–978).

Hubbell, J. T., Koch, B., & McCormick, D. (1992). Modern crane control enhancements. In *Ports' 92* (pp. 757–767). ASCE.

Idres, M., Youssef, K., Mook, D., & Nayfeh, A. (2003). A nonlinear 8-DOF coupled crane-ship dynamic model. In *44th AIAA/ASME/ASCE/AHS/ASC Structures, Structural Dynamics, and Materials Conference* (p. 1855).

Jin, Y., Wan, B., Liu, D., Peng, Y., & Guo, Y. (2016). Dynamic analysis of launch & recovery system of seafloor drill under irregular waves. *Ocean Engineering*, *117*, 321–331.

Khan, R. F. A., Rsetam, K., Cao, Z., & Man, Z. (2022). Singular perturbation-based adaptive integral sliding mode control for flexible joint robots. *IEEE Transactions on Industrial Electronics*, *70*(10), 10516–10525.

Kim, G. H., & Hong, K. S. (2019). Adaptive sliding-mode control of an offshore container crane with unknown disturbances. *IEEE/ASME Transactions on Mechatronics*, *24*(6), 2850–2861.

Kimiaghalam, B., Homaifar, A., & Bikdash, M. (1998). Using genetic algorithm for optimal crane control. In *NASA URC conference*.

Küchler, S., Mahl, T., Neupert, J., Schneider, K., & Sawodny, O. (2011). Active control for an offshore crane using prediction of the vessels motion. *IEEE/ASME Transactions on Mechatronics*, *16*(2), 297–309.

Levant, A. (2005). Quasi-continuous high-order sliding-mode controllers. *IEEE Transactions on Automatic Control*, *50(11)*, 1812–181.

Lofberg, J. (2004). YALMIP: A toolbox for modeling and optimization in MATLAB. In *2004 IEEE International Conference on Robotics and Automation (IEEE cat. no. 04CH37508)* (pp. 284–289).

Maalouf, D., Moog, C. H., Aoustin, Y., & Li, S. (2015). Classification of two-degree-of-freedom underactuated mechanical systems. *IET Control Theory & Applications*, *9*(10), 1501–1510.

Manson, G. (1982). Time-optimal control of an overhead crane model. *Optimal Control Applications & Methods*, *3*(2), 115–120.

MATLAB (2021). Symbolic maths toolbox.

Nayfeh, A. H., Ragab, S. A., & Al-Maaitah, A. A. (2002). Effect of bulges on the stability of boundary layers. *Physics of Fluids*, *31*(4), 796.

Ngo, Q. H., Nguyen, N. P., Nguyen, C. N., Tran, T. H., & Ha, Q. P. (2017). Fuzzy sliding mode control of an offshore container crane. *Ocean Engineering*, *140*, 125–134.

Olfati-Saber, R. (2001). *Nonlinear control of underactuated mechanical systems with application to robotics and aerospace vehicles* (Ph.D. thesis), Massachusetts Institute of Technology.

Palfinger NPDS series fast rescue boat davits. (2023). https://www.palfingermarine.com/en/boats-and-davits/davits/fast-rescue-boat-davits. (Accessed on 06 December 2023).

Parker, G. G., Petterson, B., Dohrmann, C., & Robinett, R. D. (1995). Command shaping for residual vibration free crane maneuvers. In *Proceedings of 1995 American Control Conference, vol. 1* (pp. 934–938). IEEE.

Pawlowski, M. (2009). Sea Spectra Revisited. In *10th International Conference on Stability of Ships and Ocean Vehicles*. St Petersberg, Russia.

Perez, T. (2006). *Ship Motion Control: Course Keeping and Roll Stabilisation Using Rudder and Fins*. Springer.

Qian, Y., Hu, D., Chen, Y., Fang, Y., & Hu, Y. (2021). Adaptive neural network-based tracking control of underactuated offshore ship-to-ship crane systems subject to unknown wave motions disturbances. *IEEE Transactions on Systems, Man, and Cybernetics: Systems*, *52*(6), 3626–3637.

Roza, A., & Maggiore, M. (2014). A class of position controllers for underactuated VTOL vehicles. *IEEE Transactions on Automatic Control*, *59*(9), 2580–2585.

Shtessel, Y., Edwards, C., Fridman, L., & Levant, A. (2014). *Sliding mode control and observation*, Birkhäuser, New York, NY.

Stilwell, D. J., & Rugh, W. J. (1999). Interpolation of observer state feedback controllers for gain scheduling. *IEEE Transactions on Automatic Control*, *44(6)*, 1225–1229.

Sun, N., Fang, Y., Chen, H., Fu, Y., & Lu, B. (2018). Nonlinear stabilizing control for ship-mounted cranes with ship roll and heave movements: Design, analysis, and experiments. *IEEE Transactions on Systems, Man, and Cybernetics: Systems*, *48*(10), 1781–1793.

Takeuchi, S., Fujikawa, H., & Yamada, S. (1988). The application of fuzzy theory for a rotary crane control. In *Proceedings. 14 Annual Conference of the Industrial Electronics Society*: *vol. 2*, (pp. 415–420).

Tuan, L. A., Lee, S.-G., Nho, L. C., & Cuong, H. M. (2015). Robust controls for ship-mounted container cranes with viscoelastic foundation and flexible hoisting cable. *Proceedings of the Institution of Mechanical Engineers, Part I: Journal of Systems and Control Engineering*, *229*(7), 662–674.

Utkin, V. I. (1992). *sliding modes in control and optimization*.

Wen, B., Homaifar, A., Bikdash, M., & Kimiaghalam, B. (1999). Modeling and optimal control design of shipboard crane. In *Proceedings of the American Control Conference*: *vol. 1*, (no. June), (pp. 593–597).

Wu, X., Xu, K., Lei, M., & He, X. (2020). Disturbance-compensation-based continuous sliding mode control for overhead cranes with disturbances. *IEEE Transactions on Automation Science and Engineering*, *17*(4), 2182–2189.

Zhang, R., & Chen, H. (2022). An adaptive tracking control method for offshore cranes with unknown gravity parameters. *Ocean Engineering*, *260*, Article 111809.

Zhang, M., Zhang, Y., & Cheng, X. (2019). Model-free adaptive integral sliding mode control for 4-DOF tower crane systems. In *2019 IEEE/ASME International Conference on Advanced Intelligent Mechatronics* (pp. 708–713).

Zhang, H., Zhao, C., & Ding, J. (2022). Online reinforcement learning with passivity-based stabilizing term for real time overhead crane control without knowledge of the system model. *Control Engineering Practice*, *127*, Article 105302.

Zhang, Y., Zhao, H., Li, G., Edwards, C., & Belmont, M. (2023). Robust nonlinear model predictive control of an autonomous launch and recovery system. *IEEE Transactions on Control Systems Technology*, *31*, 2082–2092.